Structure-Activity Relationships of the Sustained Effects of Adenosine A2A Receptor Agonists Driven by Slow Dissociation Kinetics [S]

J. Daniel Hothersall, Dong Guo, Sunil Sarda, Robert J. Sheppard, Hongming Chen, Wesley Keur, Michael J. Waring, Adriaan P. IJzerman, Stephen J. Hill, Ian L. Dale, and Philip B. Rawlins

AstraZeneca, Discovery Sciences, Alderley Park, United Kingdom (J.D.H., S.S.); AstraZeneca, Oncology, Cambridge, United Kingdom (R.J.S.); AstraZeneca, Discovery Sciences, Mölndal, Sweden (H.C.); AstraZeneca, Discovery Sciences, Cambridge Science Park, United Kingdom (I.L.D., P.B.R.); AstraZeneca, Oncology, Alderley Park, United Kingdom (M.J.W.); Leiden Academic Centre for Drug Research, Division of Medicinal Chemistry, The Netherlands (D.G., W.K., A.P.I.J.); and University of Nottingham, School of Life Sciences, United Kingdom (S.J.H.)

ABSTRACT

The duration of action of adenosine A_{2A} receptor (A2A) agonists is critical for their clinical efficacy, and we sought to better understand how this can be optimized. The in vitro temporal response profiles of a panel of A2A agonists were studied using cAMP assays in recombinantly (CHO) and endogenously (SH-SY5Y) expressing cells. Some agonists (e.g., 3cd; UK-432,097) but not others (e.g., 3ac; CGS-21680) demonstrated sustained wash-resistant agonism, where residual receptor activation continued after washout. The ability of an antagonist to reverse pre-established agonist responses was used as a surrogate read-out for agonist dissociation kinetics, and together with radioligand binding studies suggested a role for slow off-rate in driving sustained effects. One compound, 3ch, showed particularly marked sustained effects, with a reversal $t_{1/2} > 6$ hours and close to maximal effects that remained for at least 5 hours after washing. Based on the structure-activity relationship of these compounds, we suggest that lipophilic N6 and bulky C2 substituents can promote stable and long-lived binding events leading to sustained agonist responses, although a high compound logD is not necessary. This provides new insight into the binding interactions of these ligands and we anticipate that this information could facilitate the rational design of novel long-acting A2A agonists with improved clinical efficacy.

Introduction

The adenosine receptors are G protein-coupled receptors (GPCRs) that comprise four subtypes (A_1, A_{2A}, A_{2B}, and A_3) and mediate the physiologic effects of their endogenous agonist adenosine. The adenosine A_{2A} receptor (A2A) is coupled to the stimulatory G protein ($G_{\alpha s}$) and signals through cAMP pathways (Zezula and Freissmuth, 2008). A2A has a wide tissue distribution and plays many important roles such as in vasodilation, inflammation, and regulating neurotransmitter release (de Lera Ruiz et al., 2014). As a primary target of caffeine, A2A is involved in adenosine's control of wakefulness (Chen et al., 2013).

A2A is an important drug discovery target. The A2A-selective agonist regadenoson is used clinically as a pharmacological stress agent for myocardial imaging (Chen et al., 2013). A2A agonists have anti-inflammatory properties and are thus targeted for the potential treatment of chronic obstructive pulmonary disease, asthma, allergic rhinitis, sickle cell disease, and wound healing, among others, with a number of compounds (e.g., UK-432,097; compound 3cd in Table 1) reaching clinical trials (Mantell et al., 2010; Field et al., 2013). The A2A agonist BVT.115959 has also been in trials for diabetic neuropathic pain (Gao and Jacobson, 2011). Owing to its role in brown adipose activation, A2A agonism was also recently postulated as an obesity therapy (Gnad et al., 2014). Numerous potent and selective A2A agonists have been developed, and these typically maintain an adenosine structural scaffold with various substitutions on the C2 and N6 positions of the molecule (de Lera Ruiz et al., 2014) (Table 1). Crystal structures of agonist-bound A2A have been solved, providing insight into the molecular mechanisms of receptor function (Lebon et al., 2011, 2015; Xu et al., 2011).

ABBREVIATIONS: A2A, adenosine A_{2A} receptor; A2B, adenosine A_{2B} receptor; FCS, fetal calf serum; GPCR, G protein-coupled receptor; HTRF, homogenous time-resolved fluorescence; IAM, immobilized artificial membrane; K_{IAM}, immobilized artificial membrane partitioning coefficient; KRI, kinetic rate index; SAR, structure-activity relationship.

TABLE 1
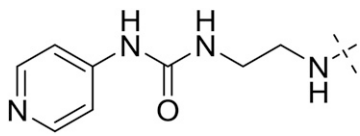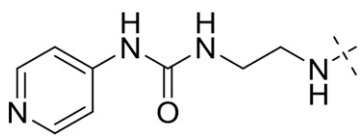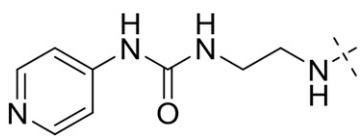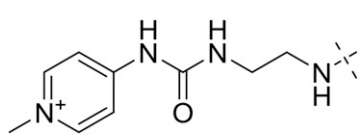Summary of the compounds investigated in this study
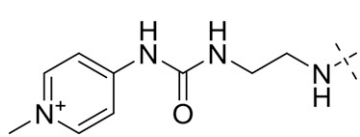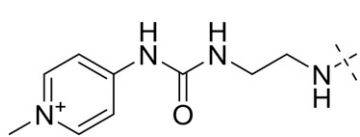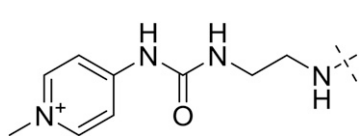
All the ligands have an adenosine scaffold, with substitution on the ribose 4 position (R1), N6 (R2), and/or C2 (R3). Otsuka-3 is an exception, because it does not share this structural scaffold. The individual structures of each compound are shown in Supplemental Fig. 1. References for compound disclosure; 1, (Marumoto et al., 1974); 2, (Bridges et al., 1987); 3, (Åstrand et al., 2015); 4, (Sato et al., 2010). AZ proprietary compounds are marked # and their synthesis is described in Supplemental Figs. 1–6.
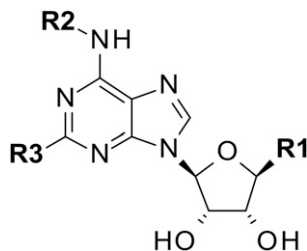
Compound number	Synonym	Ref.	R1	R2	R3
1aa	CV1808	1	H	H	
2bb	R-PIA	2	CH$_2$OH	CH(R-Me)CH$_2$Ph	H
2cb		2	CH$_2$OH	CH$_2$CHPh$_2$	H
3ab	NECA		CONHEt	H	H
3ac	CGS-21680		CONHEt	H	
3ad		#	CONHEt	H	
3cd	UK-432,097		CONHEt	CH$_2$CHPh$_2$	
3ce		#	CONHEt	CH$_2$CHPh$_2$	
3cf		#	CONHEt	CH$_2$CHPh$_2$	
3ag		#	CONHEt	H	

(continued)

TABLE 1—*Continued*

Compound number	Synonym	Ref.	R1	R2	R3
3cg		3	CONHEt	CH_2CHPh_2	
3dg		#	CONHEt	$CH_2CH(CH_3)_2$	
3eg		#	CONHEt	$CH(CH_2CH_3)_2$	
3ah		#	CONHEt	H	
3ch		3	CONHEt	CH_2CHPh_2	
3dh		#	CONHEt	$CH_2CH(CH_3)_2$	
3eh		#	CONHEt	$CH(CH_2CH_3)_2$	
4	Otsuka-3	4	*		

Duration of action is a key property for targeting a desirable clinical response profile for A2A agonists. To achieve a better safety profile, short-lived activity has been optimized for ligands developed as intravenous myocardial imaging agents (Cerqueira, 2004). On the other hand, A2A agonists developed for the treatment of chronic inflammatory diseases, such as UK-432,097, have been targeted for local drug delivery to minimize side effects (Mantell et al., 2010). A long duration of target activity alongside appropriate physicochemical properties to aid tissue retention has been suggested to help achieve efficacy through topical application (Mantell et al., 2010). Therefore, for A2A drug discovery programs it is critical to increase our understanding of the temporal response profiles of drug candidates and the mechanisms through which long/short duration of action can occur. Optimizing ligand binding kinetics has been advocated as a valuable strategy for achieving appropriate duration of action and target coverage (Copeland et al., 2006; Guo et al., 2014; Hothersall et al., 2016).

Specifically, slow A2A agonist dissociation kinetics have been cited as a potential mechanism to achieve a desirable clinical response for topically applied drugs (Mantell et al., 2010). This approach may be especially relevant for A2A where the receptor has been shown to signal without agonists inducing desensitization and internalization in recombinant systems as well as in physiologic settings (Abbracchio et al., 1992; Adami et al., 1995; Charalambous et al., 2008; Zezula and Freissmuth, 2008; Baines et al., 2011), so long-lived agonist responses are possible.

In this study, we have assessed the temporal response profiles of a range of A2A agonists in a recombinant (CHO cell) and endogenous (SH-SY5Y cell) expression system. In wash-out experiments, sustained receptor activation was observed for some, but not all, agonists tested. Our evidence points toward a predominant role for slow agonist off-rate in driving wash-resistant responses. Coupled with structure-activity relationships (SAR) for sustained effects, we can begin to define the ligand-specific binding interactions that promote

stable and long-lived binding interactions and hence persistent receptor activation.

Materials and Methods

Materials. Cell culture materials were from Life Technologies (Paisley, UK) and Sigma Aldrich (Dorset, UK). GloSensor 22F plasmid and luciferin were from Promega (Southampton, UK). Homogenous time-resolved fluorescence (HTRF) dynamic cAMP kits were from Cisbio (Codolet, France). Assay plates were from Greiner Bio One (Stonehouse, UK). Adenosine and bovine spleen adenosine deaminase (type X) were from Sigma Aldrich. Immobilized artificial membrane chromatography columns were from Regis Technologies (Morton Grove, IL). [^{3}H]ZM-241385 (specific activity 28.4 Ci/mmol) was from American Radiolabeled Chemicals Inc. (St. Louis, MO). Rolipram, CGS-21680 (2ac), NECA (3ab), and LUF5834 were from Tocris (Bristol, UK). All other compounds were synthesized at WuXi PharmaTech (Shanghai, China) or BioDuro (Beijing, China). The syntheses of new chemical entities are described in Supplemental Figs. 1–6.

Cell Culture. CHO-K1 cells were cultured in Ham's F-12 medium supplemented with 10% fetal calf serum (FCS) in an atmosphere of 5% CO_2 at 37°C. Parental CHO cells were grown in medium supplemented with 100 U/ml penicillin and 100 μg/ml streptomycin. CHO cells stably expressing human A2A (CHO-A2A) were grown in medium supplemented with 800 μg/ml G-418. CHO cells stably expressing human A2B (CHO-A2B) were grown in medium supplemented with 200 μg/ml hygromycin B. CHO cells stably expressing both human A2A and GloSensor 22F were grown in medium supplemented with 800 μg/ml G-418 and 200 μg/ml hygromycin B. HEK293 cells stably expressing human A2A (HEK-A2A) were grown in Dulbecco's modified Eagle's medium supplemented with 10% FCS, 50 μg/ml streptomycin, 50 U/ml penicillin, and 500 μg/ml G-418 in an atmosphere of 7% CO_2 at 37°C. SH-SY5Y cells were grown in a 1:1 mixture of Ham's F-12 and Dulbecco's modified Eagle's medium supplemented with 15% FCS, 1% nonessential amino acids, 1 mM L-alanyl-L-glutamine, 100 U/ml penicillin, and 100 μg/ml streptomycin in an atmosphere of 5% CO_2 at 37°C.

Real-time cAMP Assay. GloSensor 22F (Promega) was used to monitor real-time cAMP responses. CHO cells stably expressing both A2A and GloSensor 22F plasmid (clonal isolates) were seeded into white-bottomed tissue-culture treated 384-well plates at 15,000 cells per well and grown for approximately 24 hours. Culture medium was then replaced with assay buffer (Hank's buffered saline solution + 20 mM HEPES + 10% FCS + 0.8 U/ml adenosine deaminase, pH 7.4) supplemented with 612 μg/ml endotoxin-free beetle luciferin, and cells were incubated at room temperature for 2 hours. Ten times concentrated test compound was then manually added and luminescence responses measured every 3.25 minutes over the indicated time period at room temperature using an Envision plate reader (Perkin Elmer, Waltham MA). In reversal experiments, a second addition of antagonist was made in the same way.

Endpoint cAMP Assay. The endpoint cellular cAMP assay used the homogenous time-resolved fluorescence (HTRF) Dynamic competitive immunoassay kit (Cisbio), and methods were adapted from the manufacturer's instructions. Common to all endpoint experiments, after cell treatment with compound(s), a 10 μl sample was added per well to a black-bottomed 384-well plate. Dye-labeled cAMP followed by anti-cAMP antibody (5 μl/well each, diluted in lysis buffer) were then added and the plate was incubated at room temperature for 1–16 hours. To construct a standard curve, samples of known cAMP concentration were also incubated in the same way. Fluorescence was then read at 665 and 620 nm using an Envision plate-reader, and a 665/620 ratio derived. Cellular cAMP concentration was calculated by comparing these values (normalized to background fluorescence) to the standard curve for each plate.

In washout experiments, suspensions of cells were treated with compound and the cells were then physically isolated from the original treatment vessel to remove nonspecific effects of compound interactions with plastic. In 15 ml tubes, 2,400,000 cells per tube were resuspended in 100 μl of assay buffer (Hank's buffered saline solution + 20 mM HEPES + 0.01% bovine serum albumin + 0.8 U/ml adenosine deaminase, pH 7.4) containing test compound and incubated for 2 hours at 37°C. This volume was used to minimize the contact area of compound with plastic surfaces. After treatment, the buffer was then completely removed by centrifugation (two cycles of spinning at 300 g for 5 minutes to pellet cells and remove liquid) and cells were resuspended in 50 μl of fresh buffer and subsequently transferred to a fresh tube containing 12 ml of drug-free buffer. This was repeated to give three cycles of washing in three fresh tubes to remove the cells from any plastic surfaces that had been exposed to a significant concentration of test compound. Cells were incubated in the final tube for 1 hour at 37°C to allow putative dissociation of compounds from the receptor. Cells were then pelleted and resuspended in 2 ml buffer, transferred to 1.5 ml tubes, and then exposed to 40 μM rolipram (1:1 dilution of cells) for 45 minutes at 37°C to capture cAMP accumulation. Aliquots (10 μl) of each cell suspension were then added to HTRF assay plates, as described above.

For antagonist reversal experiments performed with the endpoint cAMP assay, cells adhered to collagen-coated 96-well plates were used. Cells were seeded at 20,000 cells/well (for CHO cells) or 40,000 cells/well (for SH-SY5Y cells) in culture media and grown for approximately 24 hours. Cells were then treated with test compound in 50 μl assay buffer (Hank's buffered saline solution + 20 mM HEPES + 0.8 U/ml adenosine deaminase, pH 7.4) for the indicated time. Antagonist or vehicle control was then directly added to the wells for the indicated period to follow a time course of antagonist reversal. Signaling was terminated by removing the assay buffer and replacing it with ice-cold lysis buffer (100 μl PBS + 1 M potassium fluoride + 1% Triton X-100, pH 7.00) to capture the total cellular cAMP pool at that moment in time without phosphodiesterase inhibitor. This step also served to remove putative secreted cAMP from the measurements. After incubation for >30 minutes at room temperature with shaking to extract cAMP, a sample of cell lysate (10 μl) from each well was added to a corresponding well in a HTRF assay plate.

[^{3}H]ZM-241385 Radioligand Binding Studies. Motulsky-Mahan kinetic competition binding experiments were performed by measuring the association rate of [^{3}H]ZM-241385 in the presence of test ligand in membranes prepared from HEK-A2A, as described previously for this receptor (Guo et al., 2012). To measure occupation of the binding site in washout experiments, 20 μg of membranes were incubated with test compound in a volume of 400 μl for 1 hour at 37°C. Membranes were then pelleted by centrifugation at 16,100 g for 2 minutes and resuspended in 2 ml fresh assay buffer and transferred to a fresh tube and incubated for 10 minutes on ice. This was repeated three times to wash the membranes in fresh buffer. Membranes were then resuspended in 400 μl assay buffer containing 3 nM [^{3}H]ZM-241385 and incubated for 30 minutes at 37°C to label unoccupied A2A binding sites.

Immobilized Artificial Membrane Chromatography. Immobilized artificial membrane (IAM) chromatography experiments were conducted to measure the relative phospholipophilicity (log K_{IAM}) of each of the compounds since the monolayers of phosphatidylcholine stationary phase on a silica surface effectively mimic the lipid environment found in cell membranes (Ong et al., 1995; Pidgeon et al., 1995) and as such is a parameter used to measure the partitioning of compounds to fluid membranes. Test compounds (5 μl injections of 10 mM solutions in dimethylsulfoxide) were separated on a Regis IAM PC DD2 (100 × 4.6 mm) column preceded by an IAM PC DD2 10/300 guard column, both maintained at 50°C and eluted with 50 mM ammonium acetate (pH 7.4 adjusted with ammonium hydroxide) (solvent A) and acetonitrile (solvent B) at a flow rate of 1.0 ml/min, using a linear gradient (Agilent 1200 series binary pumps, autosampler and temperature control units, Agilent Technologies Ltd., Stockport, UK). Initial conditions started at 0% B, which was increased to 100% B over 6 minutes, where it was held for a further 0.5 minute,

before returning to 0% B over the next 0.5 minute, at which it was held for a further 2 minutes before the subsequent injection. Detection was by means of ultraviolet absorption between wavelengths of 254 and 360 nm (0.1 minute peak width, 2 second response time) via an Agilent 1200 series diode array detector (Agilent Technologies Ltd.). The retention factor log K_{IAM} was obtained by calculating $\log[(t_R\text{-}t_0)/t_0]$, where t_R was the retention time of the ultraviolet peak on the gradient and t_0 the corresponding column void volume time for each acquisition ($n = 3$, average %CV = 0.17). The equilibrium partition coefficient log K_{IAM} was subsequently determined by multiplying by a chromatographic hydrophobicity index for immobilized artificial membrane chromatography at pH 7.4 (CHI $IAM_{7.4}$), the latter measured for a diverse set of β-adrenergic compounds and normalized to the values obtained previously (Sykes et al., 2014).

LogD$_{7.4}$ Measurements. Lipophilicity measurements were undertaken by calculating the distribution coefficients between 1-octanol and aqueous buffer at pH 7.4, with the system being validated using three quality control compounds (high, moderate, and low logD$_{7.4}$) and an internal standard (verapamil) all with established logD$_{7.4}$ values. Liquid transfers were performed using a Beckman robot (Beckman Biomek FX, Beckman Coulter UK, High Wycombe, UK). Four separate dilutions of all phosphate buffer and 1-octanol samples were analyzed and evaluated to arrive at the measured logD$_{7.4}$ value. Compounds in 10 mM DMSO solutions were subjected to the shake flask technique whereby equal parts of a phosphate buffer (10 mM) and 1-octanol were vigorously mixed in a separation funnel three times (at least 15 minutes between each mixing) to saturate the solutions. The mixture was left overnight to separate the upper octanol phase from the lower buffer phase before liquid chromatography (Waters Acquity UPLC, Milford, MA) separation and mass spectrometry analysis on a triple quadrupole mass spectrometer (Waters Micromass TQS running MassLynx 4.1) where the components were separated using an Waters Acquity UPLC HSS T3 1.8 μm, 2.1 × 50 mm column. Calculated logD$_{7.4}$ values were dependent on 1-octanol solubility as well as mass spectrometry responses and typical values vary between 0 and 4.

Results

Sustained Wash-resistant A2A Agonist Responses. We examined the potential for ligand-specific effects on the durability of A2A cAMP signaling in CHO-A2A cells. A panel of 18 A2A agonists were chosen from previously disclosed compounds or those from the AstraZeneca compound library, as summarized in Table 1 (individual compound structures are shown in Supplemental Fig. 1). Agonist potency was determined by concentration-response analysis (sample curves shown in Supplemental Fig. 2) using the GloSensor cAMP assay, and physicochemical properties of the compounds were also analyzed (logD$_{7.4}$ and artificial membrane partitioning co-efficient log K_{IAM}), as compiled in Table 2.

Sustained effects were investigated in washout experiments after chronic agonist treatment, as determined by residual cAMP responses that persist after removal of free agonist by infinite dilution. Because a propensity for GPCR ligands to nonspecifically interact with plastic assay plates can prevent complete washout from the experimental system and thus confound the interpretation of sustained effects (Palmgren et al., 2006; Wennerberg et al., 2010), we designed experiments to avoid this phenomenon. This was achieved by physically isolating agonist pretreated cells from their original treatment vessel. Suspensions of cells were first stimulated with test agonist in tubes (equipotent 20× EC$_{90}$ concentrations, 2 hours, 37°C), then washed three times by centrifugation and resuspension in fresh buffer, each time

TABLE 2
Summary data for A2A agonist pharmacology, physicochemical properties, and antagonist reversal rate

pEC$_{50}$ is derived from concentration-response curves using the GloSensor cAMP assay (Sample curves in Supplemental Fig. 2) measured at 20°C for 100 minutes. LogD$_{7.4}$ and log K_{IAM} are experimentally measured physicochemical properties used as indicators of, respectively, lipophilicity and membrane partitioning. Antagonist reversal $t_{1/2}$ to estimated agonist off-rate was derived from normalized antagonist reversal curves (one-phase exponential decay) shown in Fig. 3. Curves were constrained to give a minimal response of "0" as incomplete reversal observed over the time-course. Accurate reversal $t_{1/2}$ values were difficult to derive for THESE data, but we can say with confidence that $t_{1/2} > 100$ minutes. pEC$_{50}$ values and reversal half-life estimates are an average of 3 or 4 experiments performed in triplicate.

Compound	pEC$_{50}$	logD$_{7.4}$	log K_{IAM}	Antagonist Reversal t1/2 (min)
1aa	7.30 ± 0.19	0.6	1.13	5.50 ± 0.28
2bb	6.16 ± 0.13	N.T.	N.T.	8.14 ± 1.07
2cb	5.97 ± 0.19	2.6	2.31	4.48 ± 0.50
3ab	7.52 ± 0.06	−0.3	−0.57	5.80 ± 0.25
3ac	7.18 ± 0.14	< -0.8	−0.09	8.99 ± 0.19
3ad	5.70 ± 0.21	0.3	0.86	5.02 ± 0.37
3cd	8.32 ± 0.07	3.6	2.38	39.99 ± 4.41
3ce	6.74 ± 0.17	1.9	3.35	6.50 ± 0.85
3cf	5.91 ± 0.04	0.1	2.74	9.44 ± 3.28
3ag	7.53 ± 0.06	< -0.1	0.51	10.56 ± 0.91
3cg	9.04 ± 0.09	3.5	2.56	*309 ± 124
3dg	9.01 ± 0.13	1.8	1.86	38.29 ± 4.80
3eg	9.84 ± 0.05	2.25	2.08	63.34 ± 3.12
3ah	7.79 ± 0.08	< -1	0.66	11.31 ± 1.60
3ch	9.89 ± 0.10	0	2.87	*417 ± 86
3dh	9.35 ± 0.10	< -1.1	2.21	39.15 ± 9.84
3eh	9.48 ± 0.22	−0.7	2.42	*151 ± 32
4	7.93 ± 0.17	0	2.21	6.25 ± 0.72

N.T., not tested.

being transferred to a fresh tube. After a subsequent incubation in fresh buffer to allow putative dissociation of ligand (1 hour, 37°C) residual cAMP accumulation responses with the inclusion of a phosphodiesterase inhibitor (40 μM rolipram) were measured using an endpoint HTRF assay. Parallel compound pre-treated cells were also subsequently directly exposed to a maximal concentration (20× EC$_{90}$) of the A2A agonist UK-432,097 (compound 3cd) during the phosphodiesterase inclusion period to determine acute receptor responsiveness.

Cells pretreated with 3cd, 3ce, 3cg, 3dg, 3eg, 3ch, 3dh, and 3eh demonstrated significantly increased cAMP accumulation compared with cells pretreated with vehicle control ($P < 0.05$, 0.01, or 0,001; ANOVA Dunnett's posttest; $n = 3$–5; Fig. 1A). In contrast, the effects of 1aa, 2bb, 2cb, 3ab, 3ac, 3ad, 3cf, 3ag, 3ah, and 4 were readily removed by washing as pre-exposure with these compounds did not elicit a residual response and cellular cAMP levels returned to baseline (Fig. 1A). Therefore, sustained wash-resistant agonism occurred for some, but not all, of the compounds tested, highlighting the potential for ligand-specific factors that can regulate duration of action. The magnitude of residual postwash responses relative to maximal receptor activation measured by direct exposure to agonist was varied, with 3cg, 3ch, and 3eh pretreated cells reaching >70%, whereas 3cd, 3dg, and 3eg pretreated cells were limited to <25% (Fig. 1A).

Further experiments investigated the wash-resistant effects of compounds 3cd and 3ch in more detail. Concentration-response analysis was performed by measuring postwash cAMP responses after pretreatment with a concentration range of each compound (2 hours, 37°C) followed by a 1-hour recovery period. These analyses (Fig. 1B) yielded an EC$_{50}$ of
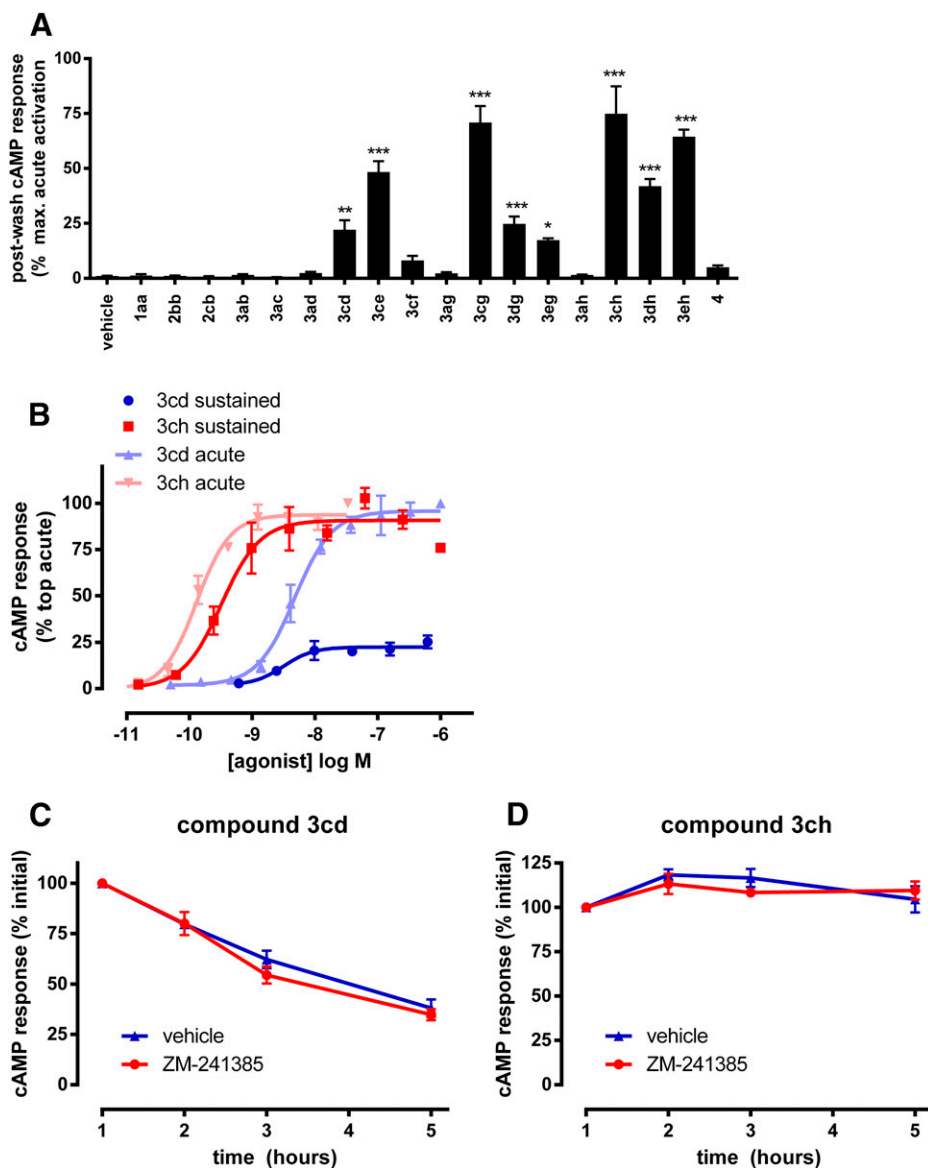
Fig. 1. Sustained wash-resistant A2A agonist response measured by physically isolating agonist pre-treated cells from the original treatment vessel. (A) Cells were pre-treated with $20\times EC_{90}$ concentrations of each agonist for 2 hours before washout and incubation in drug-free buffer for 1 hour (37°C) and measurement of cAMP capture by subsequent inclusion of rolipram. Sustained cAMP responses are normalized to acute responses ($20\times EC_{90}$ of 3cd) measured in parallel in the same population of pre-treated cells. *$P < 0.05$, **$P < 0.01$; ***$P < 0.001$ determined by ANOVA with Dunett's post-test compared with vehicle control pretreated cells. (B) Concentration-responses analysis of postwash residual effects of 3cd (blue circles) and 3ch (red squares). Cells were pretreated with the indicated concentrations of agonist before residual cAMP response measured after washout. Responses are normalized to acute responses by direct application of 3cd. For direct comparison, the acute pharmacological responses of 3cd (light blue triangles) and 3ch (light red triangles) in the GloSensor cAMP assay are shown alongside. (C and D) Time course of sustained responses after pretreatment with EC_{90} concentrations of 3cd (C) or 3ch (D) after washout, with (red circles) or without (blue triangles) subsequent inclusion of antagonist (100 nM ZM-241385) for the indicated time. Responses are normalized to responses measured at 1 hour postwash. Data represent an average ± S.E.M. of 3–5 experiments performed in triplicate.

3.13 ± 3.99 and 0.31 ± 0.07 nM for 3cd and 3ch, respectively, which were well matched to potency values estimated with direct (no wash) stimulation of the receptor (Fig. 1B; Table 2). The postwash concentration-response curves also yielded E_{max} values for 3cd and 3ch, respectively, of 25.59 ± 6.32 and 93.03 ± 8.55% of responses achieved with direct maximal receptor activation, further confirming the difference between these ligands in the magnitude of sustained wash-resistant responses.

Next, the durability of postwash responses after application of a single concentration (EC_{90}) of each agonist were compared in time course experiments over a 5-hour recovery period (at 37°C) (Fig. 1, C and D). Parallel agonist pretreated cells were also exposed to excess A2A antagonist (100 nM ZM-241385) after washout over this time to investigate ligand rebinding, because this is a potential mechanism for prolonged receptor effects (Vauquelin and Charlton, 2010). Washing alone causes "infinite dilution" of unbound ligand and thus any ligand that remains is either receptor bound or capable of rebinding (i.e., not effectively removed from the vicinity of the receptor). The

same is true for washing plus antagonist, although the effect of rebinding is removed because free receptor sites are occupied and only prebound agonist can evoke a response. Responses to 3cd were gradually lost over a number of hours, although 38.01 ± 7.37% of initial responses still remained after 5 hours (Fig. 1C). Because there was little effect of antagonist, rebinding does not play a role, suggesting instead that slow dissociation kinetics are the primary cause for slow loss of response. This is consistent with the drop in E_{max} alongside minimal change in potency in postwash concentration-response curves because for each applied concentration there is a time-dependent decrease in response but the relative difference in effect between the applied concentrations is preserved because dissociation rate is concentration independent. In contrast, responses to 3ch were markedly stable, with little loss of receptor function observed after 5 hours and no effect of antagonist (Fig. 1D). This observation, coupled with the lack of change in potency or maximal effect in postwash concentration-response curves suggests that the sustained effect of 3ch is predominantly a consequence of preformed

binding events that persist over the time course of the experiments because of a very slow off-rate.

GloSensor Reversal Assay to Estimate Agonist Dissociation Kinetics. The most straightforward explanation for sustained wash-resistant agonist responses is slow ligand dissociation kinetics (Hothersall et al., 2016). We therefore assessed agonist off-rates using the real-time GloSensor cAMP assay by monitoring antagonist mediated reversal of pre-established agonist responses. Based on the notion that antagonist reversal involves competitive displacement of agonist molecules and therefore requires agonist dissociation, reversal rate is a surrogate read-out for agonist dissociation rate (explained pictorially in Fig. 2A). This offers a novel, straightforward, and relatively high-throughput methodology to investigate agonist binding kinetics in whole cells.

Cells were incubated with equipotent concentrations of agonist (EC_{90}), and real-time responses were measured at room temperature until a relatively stable plateau response was reached (100 minutes). Excess antagonist (100 nM ZM-241385) or vehicle was then directly added and subsequent responses continually measured. Sample traces for 1aa and 3cd are shown in Fig. 2, B and C and illustrate that, upon antagonist addition, cAMP responses decreased to baseline levels, consistent with complete displacement of agonist. Comparing the traces for these two compounds shows clear differences in reversal rate, consistent with differential dissociation kinetics.

To quantify reversal rates, responses in antagonist-treated cells were normalized to vehicle control at each time point (% VEH) and nonlinear regression (one-phase exponential decay) was performed. The reversal traces (Fig. 3) and best-fit reversal $t_{1/2}$ values (Table 2) for our agonist panel revealed strong ligand-specific differences. 3cg, 3ch, and 3eh had very slow apparent kinetics, with incomplete reversal over the measurement time course. Accurate reversal half-lives were therefore hard to quantify for these compounds, although we can state with confidence that they were greater than 200 minutes. 3cd, 3dg, 3eg, and 3dh were completely reversed by antagonist but still had slow reversal rates with $t_{1/2} > 38$ minutes. The remaining compounds showed rapid reversal with $t_{1/2}$ values < 11.5 minutes, and the most rapidly reversed compound was 2cb ($t_{1/2} = 4.48 \pm 0.50$ minutes).

Importantly, ZM-241385 was able to competitively antagonize agonist responses in this assay when cells were preincubated with the antagonist before addition of 3cd or 3ch at relevant concentrations (Supplemental Fig. 3, A and B), demonstrating that a slow or absent reversal effect is not due to an inability of ZM-241385 to antagonize the responses. Moreover, consistent results were obtained when the endpoint cAMP assay was used to measure reversal rates (Supplemental Fig. 3, C and D), suggesting that the GloSensor system is an accurate measure of cellular cAMP fluxes.

In general, agonists that displayed sustained wash-resistant effects were characterized by slow GloSensor reversal rates, which further supported our hypothesis that persistent responses can be driven by slow dissociation kinetics. There appeared to be a hyperbolic relationship between GloSensor reversal rates and the magnitude of wash-resistant responses determined with equipotent agonist concentrations. We therefore examined the relationship between the $\log t_{1/2}$ values and postwash responses and observed a linear relationship with a reasonable correlation ($r^2 = 0.73$;
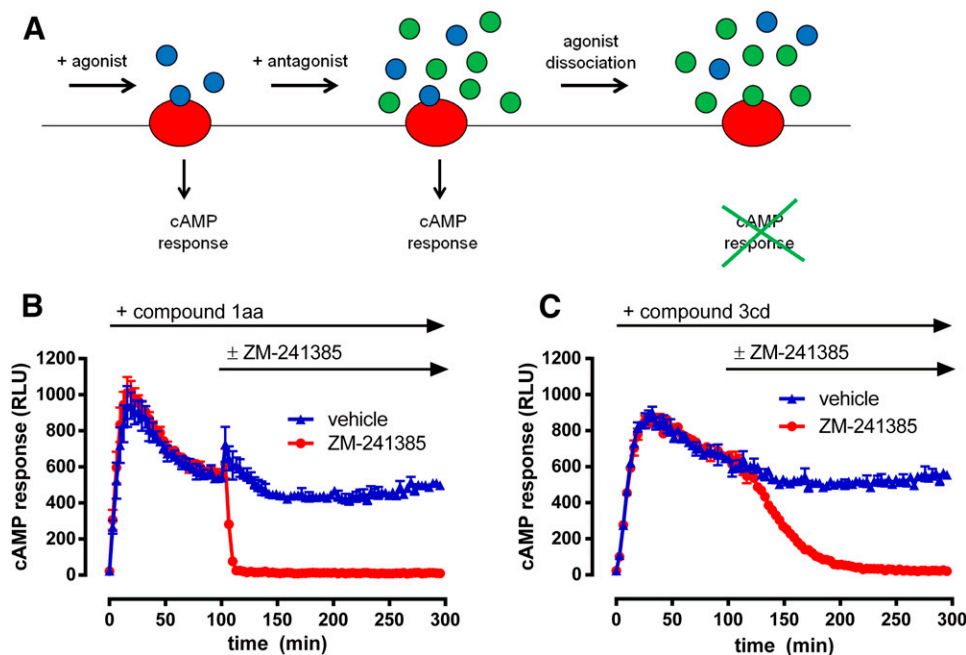
Fig. 2. Explanation and demonstration of the GloSensor reversal assay used to estimate agonist dissociation rate. (A) Schematic cartoon describing the system. Cells are first incubated with agonist (blue circles) to permit assumed equilibrium binding to receptors (red circles), which generates a relatively stable cAMP response. Excess antagonist (green circles) is then directly added to the cells. Upon dissociation of the agonist from the receptor, antagonist then occupies the binding site and prevents further activation by the agonist. This causes cessation of cAMP responses, at a rate that is dependent upon agonist dissociation kinetics. (B and C) Sample GloSensor reversal traces for 1aa (B) and 3cd (C) demonstrate that reversal rate is agonist dependent. Upon incubation of agonist (EC_{90}) and generation of relatively stable cAMP responses for 100 minutes, addition of vehicle control (blue triangles) has little effect on responses for a further 200 minutes. However, addition of antagonist at 100 minutes (red circles; 100 nM ZM-241385) causes a complete reversal of cAMP response to basal levels. 1aa reversal is faster, consistent with a more rapid off-rate compared with 3cd. Data represent an average of three experiments performed in triplicate.
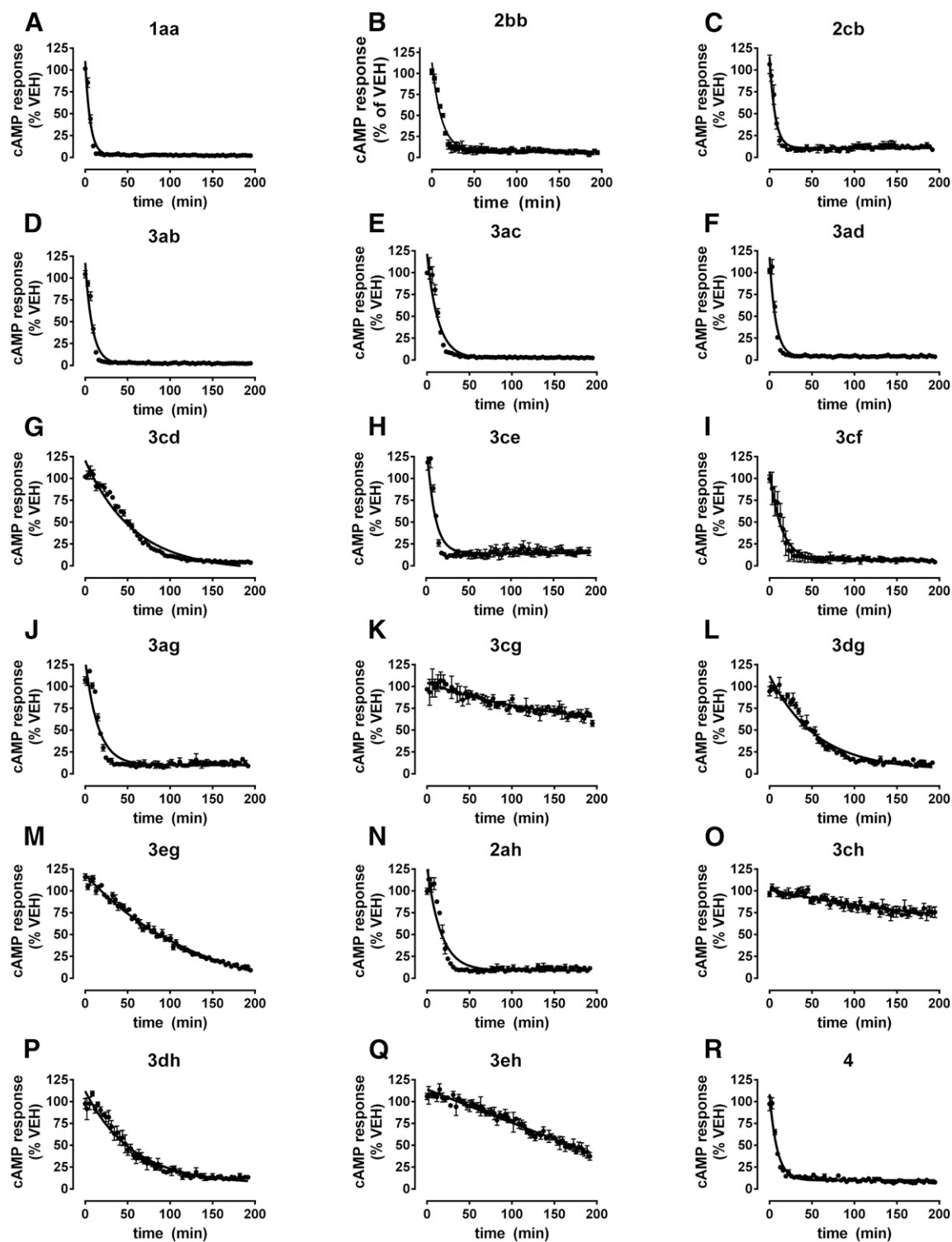
Fig. 3. Normalized GloSensor reversal traces for a sample of eighteen A2A agonists at 20°C. (A–R) Stable responses were generated to each agonist applied at an EC_{90} concentration (100 minutes, 20°C) before antagonist (100 nM ZM-241385) or vehicle was applied for 200 minutes (20°C). Data points represent antagonist-treated responses expressed as a percentage of vehicle control for each time point to display reversal rate traces over the postantagonist period. Best-fit lines represent nonlinear regression one-phase exponential decay from the average ± S.E.M. of three experiments performed in triplicate. For example, plots (C) and (D) represent normalized data from Figs. 2B and 4C, respectively.

$P < 0.0001$; $n = 18$ ligands; Fig. 4). Compound 3ce was a clear outlier in this analysis because it has a sustained effect but is rapidly reversed by the antagonist, and when removed the correlation improved greatly ($r^2 = 0.89$). Intriguingly, the rapid reversal of 3ce was unique to experiments that used ZM-241385, because an alternative reversal agent, LUF5834, was unable to fully reverse 3ce-mediated responses, which would thus categorize 3ce as a slowly dissociating compound,
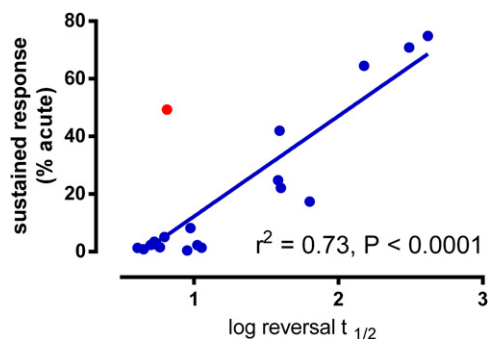
Fig. 4. Correlation of sustained wash-resistant agonist responses and the reversal rates of agonists in the GloSensor assay. Linear regression plot of log converted reversal $t_{1/2}$ values (from Table 2) against sustained responses (from Fig. 1A above). Compound 3ce is represented as a red circle, to highlight that is an outlier. Data from Table 2 is plotted on the x-axis and data from Fig. 1A is plotted on the y- axis.

Fig. 5. [^{3}H]ZM-241385 binding experiments. (A) Washout experiments to investigate the persistence of binding site occupation by A2A agonists. HEK-A2A membranes were incubated with 1aa, 3cd, 3eg, 3ch, or 4 (1 μM, 1 hour, 37°C) before washing. Membranes were then incubated with [^{3}H]ZM-241385 (30 minutes, 37°C) before separation of unbound radioligand by vacuum filtration. *$P < 0.05$, **$P < 0.01$; ***$P < 0.001$ repeated-measure ANOVA with Dunnett's post-test compared with untreated binding signal. (B) [^{3}H]ZM-241385 association rate measured at room temperature under control conditions (green squares) or in the presence of 350 nM 3cd (blue triangles) or 120 nM 3ch (red circles).

as expected from washout experiments (Supplemental Fig. 4A). This anomaly in our data set may point toward a probe-dependent allosteric interplay between 3ce and ZM-241385 binding and/or function. Indeed, the remaining ligands in our panel showed good correlation between reversal rates derived using the two alternative reversal agents, with 3ce being unique in its ability to discriminate between antagonists (Supplemental Fig. 4E).

Radioligand Binding to Investigate the Kinetics of A2A Agonists in Membranes from HEK-A2A Cells. To further investigate a role for agonist off-rate in driving sustained responses, we monitored occupation of the A2A binding site after washout in radioligand binding experiments with [^{3}H]ZM-241385 using a fresh tubes approach equivalent to our functional studies (Fig. 5A). Membranes from HEK-A2A cells pretreated with 3cd, 3eg, or 3ch (1 μM, 1 hour, 37°C) had significantly fewer available binding sites after washing than control untreated membranes ($P < 0.05$, 0.01, or 0.001 ANOVA with Dunnett's posttest; $n = 3$), consistent with an inability to remove these ligands by washing and persistent occupation of the binding site over this time course. In contrast, 1aa, which represents an exemplar ligand without a sustained response and that is rapidly reversed by antagonist, was readily removed from the binding site by washing ($P < 0.05$ compared with vehicle control; ANOVA with Dunnett's posttest; $n = 3$). Together these findings corroborate our cAMP reversal data and identify persistent ligand binding as an important factor for sustained effects.

We next sought to quantify A2A agonist binding kinetics using the Motulsky-Mahan competition radioligand binding with [^{3}H]ZM-241385, as described previously for this receptor (Guo et al., 2012). Initial experiments performed at 4°C yielded residence time estimates (Supplemental Fig. 5, A and B). However, discrepancies between these values and our functional cAMP data suggested that low temperature may have caused an underestimation of residence time. Kinetic experiments were therefore performed at room temperature. Although accurate estimation of residence time is technically challenging at increased temperature, we were able to calculate a kinetic rate index (KRI), which offers a qualitative assessment of binding kinetics (Guo et al., 2013) (Fig. 5B). KRI analysis showed that 3cd and 3ch have long residence times
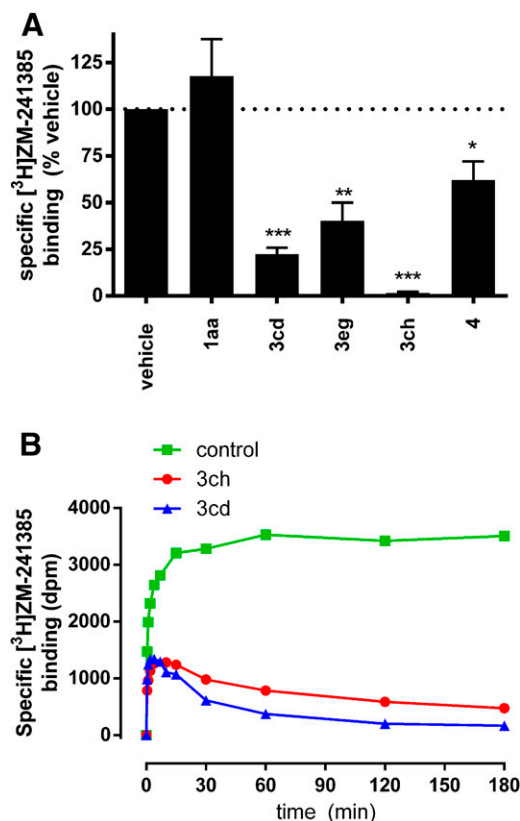
with respective KRI values of 6.4 and 2.6, and both causing characteristic "overshoot" in [^{3}H]ZM-241385 association curves. In summary, radioligand binding studies confirm that 3cd and 3ch have slow A2A dissociation kinetics, although the rank order of estimated off-rate is different to the functional reversal rates and may point to subtleties in the ability of these two indirect techniques to determine binding kinetics. Importantly, our data do not support a role for a change in cell background, the use of isolated membranes or a different buffer system in influencing these discrepancies (Supplemental Fig. 5, C–E).

Adenosine Receptor Specificity of Sustained Agonism. A selection of compounds were profiled at the adenosine A2B receptor using a stable CHO-A2B cell line of the same parental background, at which they demonstrated robust cAMP stimulation responses (Supplemental Fig. 6). cAMP responses to 3ab, 3cd, 3eg, and 3ch (EC$_{90}$ for A2B) were rapidly reversed by antagonist (2 μM ZM-241385) with $t_{1/2} < 3$ minutes measured in the endpoint cAMP assay (Fig. 6A). Furthermore, sustained wash-resistant agonist responses were either absent (3ab and 3cd) or very weak (3eg and 3ch) at A2B (Fig. 6B). Together, these findings indicate that the slow dissociation kinetics and robust sustained agonism of these compounds are not evident at A2B, being instead A2A-specific
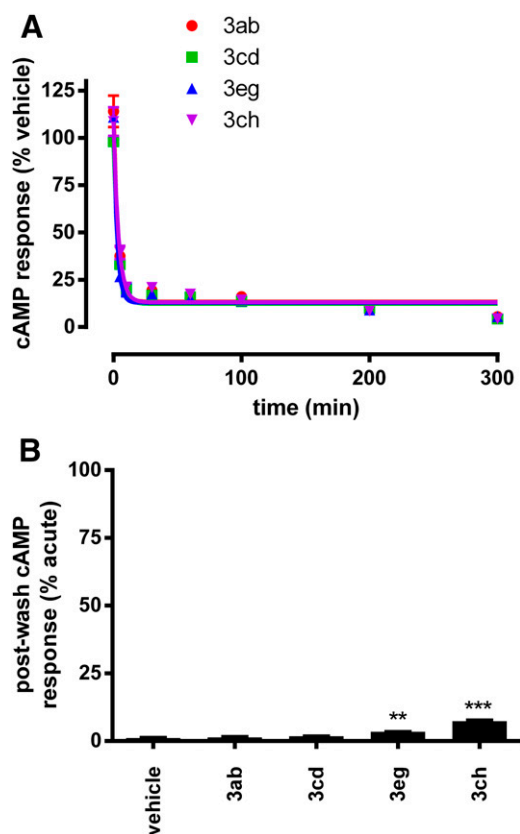
Fig. 6. Investigating the effect of some A2A agonists at the A2B receptor. (A) Antagonist reversal of agonists at A2B using the endpoint cAMP assay. CHO-A2B cells were incubated with EC_{90} (at A2B) concentrations of 3ab (red), 3cd (green), 3eg (blue), or 3ch (purple) for 2 hours at room temperature before addition of antagonist (2 μM ZM-241385) or vehicle for the indicated times. Data points represent antagonist-treated cAMP responses normalized to vehicle control at each time point. Best-fit lines represent nonlinear regression one-phase exponential decay from an average $\pm$ S.E.M. of three experiments performed in triplicate. (B) Sustained agonism at in CHO-A2B cells. Sustained cAMP responses were measured in washout experiments, measuring residual cAMP responses after pretreatment of CHO-A2B cells with EC_{90} concentrations of 3ab, 3cd, 3eg, and 3ch. cAMP responses are normalized to acute responses ($20\times$ EC_{90} of NECA) measured in parallel in the same population of pretreated cells. **$P < 0.01$; ***$P < 0.001$ as determined by repeated-measure ANOVA with Dunnett's post-test compared with responses in vehicle control pretreated cells. Data represent an average of three experiments performed in triplicate.

phenomena. This suggests a predominant role for the receptor binding site rather than non-specific effects of the cellular/experimental system.

A2A Agonist Temporal Response Profiles in an Endogenous Expression System. To validate the physiologic relevance of our findings, we also investigated A2A agonist responses in an endogenous receptor expression system. Human neuroblastoma SH-SY5Y cells were used as these demonstrated robust and predominantly A2A-mediated cAMP responses, based on the high potency of 1aa, 3cd, and 3ch, and their sensitivity to an A2A-selective antagonist (Supplemental Fig. 7). In time-course experiments, cells were stimulated with these agonists (at an EC_{90} concentration as determined in SH-SY5Y cells, 100 minutes) before direct addition of either vehicle control or antagonist (100 nM ZM-241385) and incubation for a time course over 3 hours (Fig. 7, A–F). When performed at room temperature (Fig. 7, A,

C, and E), these time courses were consistent with data from our recombinant expression system; agonist responses were stable over time in control (no antagonist) treatment. Antagonist addition reversed the responses rapidly for 1aa (complete reversal within the earliest time-point), slowly for 3cd (approximate t1/2 of 1 hour), and had little effect on 3ch, highlighting differences in their off-rates that agree with GloSensor reversal data in our recombinant cell line. When performed at 37°C (Fig. 7, B, D, and F), some interesting differences with our CHO-A2A system were observed as agonist responses were less stable over time in control time courses, with gradual reduction in cAMP levels to baseline levels. Despite this, enough response window remained to observe antagonist-mediated reversal after 1 and 2 hours, where and 1aa and 3cd were significantly reversed, whereas 3ch remained unaffected. Thus, 3ch appears to have a slow off-rate at physiologic temperature in these cells. However, these findings suggest that in some cell backgrounds, cellular mechanisms that dampen receptor responses over time may limit the long duration of action of sustained compounds at 37°C. Multiple functionally and temporally distinct mechanisms have been shown to cause agonist-driven dampening of A2A responses (Chern et al., 1993, 1995; Palmer et al., 1994). We speculate that SH-SY5Y cells are more susceptible to a gradual loss of A2A responsiveness because they are better equipped than CHO cells with the cellular machinery involved in the downregulation of receptors and/or signaling proteins. Nevertheless, robust responses remain intact for a number of hours of chronic agonist stimulation in SH-SY5Y cells, and the rapid desensitization profile typical of GPCRs is not observed, offering the opportunity for prolonged agonist effects.

The ability of these compounds to display sustained wash-resistant agonist responses was investigated in SH-SY5Y cells with a 1 hour postwash recovery time at 37°C (Fig. 7G). Cells pretreated with 3ch had significantly elevated residual cAMP response after washout compared with control ($P < 0.01$; ANOVA with Dunett's post-test; $n = 3$), confirming that cell/receptor-mediated sustained agonism could occur at the endogenously expressed receptor. Cells pre-exposed to 1aa or 3cd did not have increased residual cAMP responses. That postwash responses are absent in 3cd pretreated cells may point toward the weak sustained effects of this compound being compounded by loss of function by downregulation of overall receptor responsiveness. Indeed, wash-resistant responses to 3cd (and 3ch) could be observed at room temperature where downregulation is not pronounced (Fig. 7H). In summary, cell-specific factors can influence persistent agonist responses.

Discussion

In this study we investigated the in vitro temporal response profiles of a panel of A2A agonists. Because there is good evidence for the clinical relevance of the duration of action of these drugs, we sought to better understand the mechanisms behind these properties. Our data show that some agonists can continue to activate the receptor for at least a number of hours after removal of free ligand by infinite dilution, whereas others are readily removed by washing. This suggests that certain ligand-specific properties can regulate duration of action after washing and confer sustained agonism. Similar phenomena have been observed for a growing number of
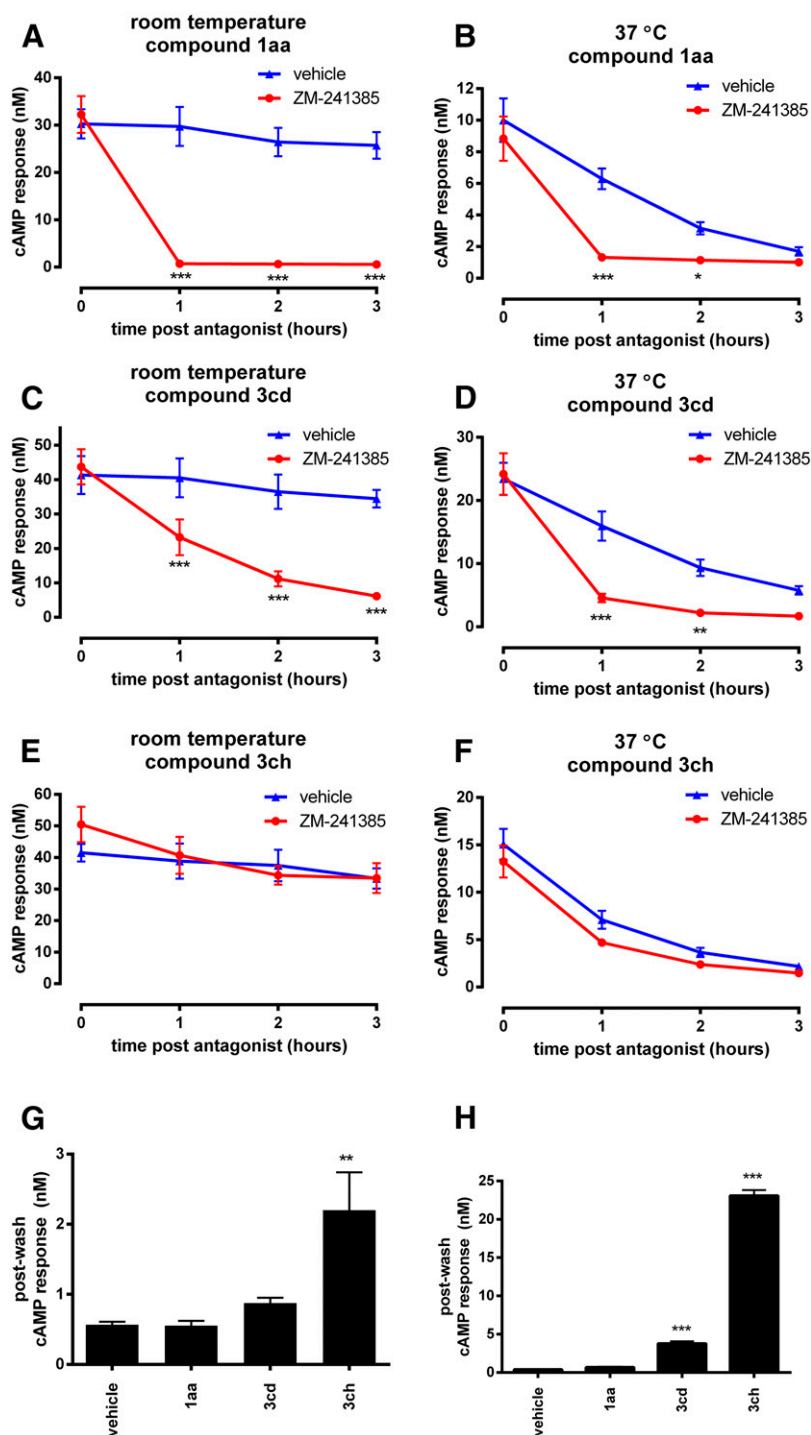
Fig. 7. Temporal response profiles of A2A agonists at endogenously expressed receptors in SH-SY5Y cells using the endpoint cAMP assay. (A–F) Time course experiments determining agonist responses stability and the ability of an antagonist (100 nM ZM-241385) to reverse these. Experiments were performed at either room temperature (A, C, E) or 37°C (B, D, F). Cells were incubated with EC_{90} concentrations of 3cd (A, B), 3ch (C, D), or 1aa (E, F) for 100 minutes, before direct addition of antagonist (red) or vehicle (blue) in a 1:10 dilution and further incubation for the indicated times, followed by direct addition of rolipram (in a 1:1 dilution) for 45 minutes. $*P < 0.05$; $**P < 0.01$; $***P < 0.001$ as determined by repeated-measure ANOVA with Bonferroni's post-test comparing antagonist versus vehicle treated responses for the each time point. (G–H) Sustained agonist responses measured in washout experiments. Suspensions of SH-SY5Y cells were pre-treated with $20\times$ EC_{90} concentrations of each agonist (2 hours) at 37°C (G) or room temperature (H) before washout and recovery in drug-free buffer for 1 hour (37°C) and measurement of cAMP capture by subsequent inclusion of rolipram at the relevant temperature. $**P < 0.01$; $***P < 0.001$ determined by repeated-measure ANOVA with Dunnett's post-test compared with vehicle control.

GPCR agonists, although it is often challenging to determine the precise mechanisms through which this occurs (Hothersall et al., 2016).

We hypothesized that either slow dissociation kinetics or rebinding of agonist molecules could drive sustained responses and sought to delineate these mechanisms by examining the ability of an antagonist to interrupt agonist responses. Rebinding can allow multiple sequential short-lived binding events, whereas slow kinetics involve singular long-lived binding events, meaning that only the former is susceptible to antagonist reversal effects as the agonist

dissociates to leave free binding sites. Together, our findings are consistent with A2A agonist duration of action in cellular experiments that is governed by their dissociation kinetics from cell surface receptors. In other words, after washing, predominantly receptor-bound agonist remains, and responses are lost as a function of the rate at which agonist/receptor complexes dissociate. This is supported by the following pieces of evidence:

1. Sustained agonists were characterized by slow antagonist reversal rates, and there is a correlation between reversal rate and the magnitude of sustained agonism (Fig. 4).

2. Radioligand binding experiments suggest that sustained A2A agonists persistently occupy the binding site after washout. Moreover, sustained agonists have a long residence time, whereas a readily washed ligand has rapid kinetics.

3. Little/no potency is lost when comparing postwash agonist concentration responses with their direct acute receptor stimulation (Fig. 1B). This indicates that we are measuring the same ligand/receptor interactions in both cases, instead of a requirement for a pool of nonreceptor-bound ligand that is resistant to washing (i.e., rebinding).

4. Sustained agonist responses are largely insensitive to antagonist reversal (Fig. 1, C and D), suggesting that a single stable binding event rather than rebinding mediates postwash responses.

5. Sustained agonist responses are specific for A2A and are greatly reduced at A2B, whereas the slowly dissociating profile of such ligands is lost at A2B. This strongly suggests that it is the A2A binding site rather than the cellular background that is driving the effect and is thus specific to the pharmacology of ligand/A2A interactions (i.e., agonist off-rate). Rebinding-type mechanisms would be expected to be target-independent, being a product of the ligand diffusion limitations in that system.

There is precedent for slow agonist dissociation kinetics regulating a long agonist duration of action at multiple GPCRs (Haskell-Luevano et al., 1996; Ferrandon et al., 2009; Andreassen et al., 2014; Hothersall et al., 2015; Nishiyama and Hirai, 2015). Our findings are also consistent with previous observations that the irreversibly binding A2A agonist DITC-APEC can exert sustained activation in intact tissue that cannot be reversed by antagonist (Niiya et al., 1993). Clearly, persistent agonist responses will be facilitated by a low level of receptor regulatory processes that normally serve to dampen receptor responsiveness (Hothersall et al., 2016). Indeed, a lack of desensitization and internalization as was previously demonstrated for A2A (Zezula and Freissmuth, 2008), although other investigators have observed agonist-driven loss of A2A responsiveness, which points toward an important role for cellular context (Chern et al., 1993, 1995; Palmer et al., 1994). In endogenously expressing SH-SH5Y cells we do observe a slow loss of A2A function that imparts some limit on agonist effects over a number of hours. Importantly, in a number of physiologically relevant settings (Abbracchio et al., 1992; Niiya et al., 1993; Koshiba et al., 1997), including in vivo (Adami et al., 1995), A2A agonist responses have been shown to be stable over time. Thus, a good understanding of receptor regulatory processes in target tissues will be crucial to fully understand and characterize the clinical profile of GPCR agonist drugs.

There is a burgeoning understanding of SAR that underpins the binding kinetics of GPCR ligands, which is anticipated to benefit greatly drug discovery. The sustained A2A agonists identified in this study are characterized by lipophilic N6 substitutions as well as bulky C2 substituents, and wash-resistant responses are lost when these groups are removed or replaced (structures shown in Table 1 and washout data summarized in Fig. 1A). When the N6 group is removed from sustained compounds (as in 3cd to 3ad, 3cg to 3ag, or 3ch to 3ah) wash resistance is lost and reversal rate is greatly accelerated. Modifying the N6 group also influences these kinetics parameters (as evidenced by differences between 3ch, 3dh, and 3eh, as well as 3cg, 4dg, and 3eg). Equally, when the N6 group is maintained but the C2 is removed, sustained responses are absent (compound 2cb), and modifying the C2 group of N6 substituted compounds greatly influences kinetic parameters (compare the responses to 3cd, 3ce, 3cf, 3cg, and 3ch). Therefore, both N6 and C2 groups contribute to binding kinetics, and the appropriate substitution of both within the same molecule is required for persistent receptor activation.

With the benefit of a wealth of published structural biology data for A2A, we were able to predict the manner in which agonist interactions in the binding pocket might confer slow off-rate. Comparing the crystal structures of A2A bound to the substituted agonist 3cd (UK-432,097) (Xu et al., 2011) and the unsubstituted agonist 3ab (NECA) (Lebon et al., 2011), it is clear that N6/C2 substituents of the UK-432,097 molecule make unique interactions with the receptor. Accordingly, modeling studies have identified three main "subpockets" within the A2A binding site that, respectively, interact with the adenosine core, the N6, and the C2 parts of UK-432,097, with the latter two being empty with unsubstituted ligands (Deflorian et al., 2012). Furthermore, molecular dynamics simulations suggest that UK-432,097 influences receptor conformational space quite differently to adenosine (Lee and Lyman, 2012). We propose a model whereby concurrent strong interactions within both the hydrophobic N6 pocket and C2 pocket hold the adenosine core of the agonist tightly in the A2A binding site to promote stable slowly dissociating ligand/receptor complexes and hence persistent activation. It is feasible that the loss of sustained responses of C2/N6 substituted compounds at the closely related A2B receptor are due to differences in accommodation of the A2B binding pocket for these groups. Indeed, the tyrosine[271] residue of A2A is important for C2-substituent binding interactions (Deflorian et al., 2012), and this is changed to asparagine in A2B, consistent with a prominent role of this group in regulating duration of binding. Modeling studies alongside receptor mutagenesis will be an exciting avenue to validate this hypothesis and help fully understand compound SAR.

The N6 substituents of the sustained compounds confer lipophilicity (high $logD_{7.4}$) and/or membrane partitioning properties (high $log K_{IAM}$) (Table 2). Interestingly, $log K_{IAM}$ and $logD_{7.4}$ can change independently of each other across related compounds. For example, comparing 3ch and 3cg the quaternization of the pryridine nitrogen in the C2-substituent of the former to form a methylpyridinium salt causes a large drop in $logD_{7.4}$ (from 3.5 to 0), whereas $log K_{IAM}$ is increased (from 2.56 to 2.87). Although we originally hypothesized that membrane partitioning ($log K_{IAM}$) might be a mechanism for sustained responses, as has been suggested for other GPCR agonists (Teschemacher and Lemoine, 1999; Austin et al., 2003; Hothersall et al., 2015), this does not appear to drive the persistent activity of the compounds tested here because the evidence listed above for slow dissociation kinetics generally excludes this phenomenon. Overall compound lipophilicity (high $logD_{7.4}$) is not a prerequisite for sustained agonism, but our data suggest that lipophilic N6 substituents in particular

are important in conferring stable binding interactions. For example, 3ch is amphiphilic and charged but contains a highly lipophilic biphenyl N6 substituent that appears to interact favorably with the chemistry of the N6 subpocket to help promote a sustained response. This highlights that high lipophilicity $logD_{7.4}$ is not required for slow dissociation and that specific local interactions have more of an influence.

In summary, we show that slow dissociation kinetics can control the duration of action of A2A agonists in a cellular setting. We suggest that key regions within the A2A binding pocket underlie this effect and that N6 and C2 substituted compounds similar to UK-432,097 (3cd) achieve stable binding by interacting with these. Whereas this stable binding effect is clearly evident in UK-432,097, it is greatly enhanced by modifying the C2 group for compounds such as 3cg and 3ch. It is tempting to speculate that this could offer a means to improve the clinical pharmacology of A2A ligands by extending duration of action. We anticipate that this SAR will prove valuable information for drug discovery at this target by informing the rational design of novel A2A agonists for optimized effect duration and improved pharmacotherapeutic profiles.

Authorship Contributions

Participated in research design: Hothersall, Guo, Sarda, Chen, Waring, IJzerman, Hill, Dale, and Rawlins.

Conducted experiments: Hothersall, Guo, Sarda, and Keur.

Contributed to reagents or analytic tools: Hothersall, Guo, Sarda, Chen, and Waring.

Performed data analysis: Hothersall, Guo, Sarda, and Chen.

Wrote or contributed to the writing of the manuscript: Hothersall, Guo, Sarda, Sheppard, Chen, Waring, IJzerman, and Rawlins.

References

Abbracchio MP, Fogliatto G, Paoletti AM, Rovati GE, and Cattabeni F (1992) Prolonged in vitro exposure of rat brain slices to adenosine analogues: selective desensitization of adenosine A1 but not A2 receptors. *Eur J Pharmacol* **227**: 317–324.

Adami M, Bertorelli R, Ferri N, Foddi MC, and Ongini E (1995) Effects of repeated administration of selective adenosine A1 and A2A receptor agonists on pentylenetetrazole-induced convulsions in the rat. *Eur J Pharmacol* **294**: 383–389.

Andreassen KV, Hjuler ST, Furness SG, Sexton PM, Christopoulos A, Nosjean O, Karsdal MA, and Henriksen K (2014) Prolonged calcitonin receptor signaling by salmon, but not human calcitonin, reveals ligand bias. *PLoS One* **9**:e92042.

Åstrand ABM, Lamm Bergström E, Zhang H, Börjesson L, Söderdahl T, Wingren C, Jansson A-H, Smailagic A, Johansson C, Bladh H, et al. (2015) The discovery of a selective and potent A2a agonist with extended lung retention. *Pharmacol Res Perspect* **3**:e00134.

Austin RP, Barton P, Bonnert RV, Brown RC, Cage PA, Cheshire DR, Davis AM, Dougall IG, Ince F, Pairaudeau G, et al. (2003) QSAR and the rational design of long-acting dual D2-receptor/beta 2-adrenoceptor agonists. *J Med Chem* **46**: 3210–3220.

Baines AE, Corrêa SA, Irving AJ, and Frenguelli BG (2011) Differential trafficking of adenosine receptors in hippocampal neurons monitored using GFP- and superecliptic pHluorin-tagged receptors. *Neuropharmacology* **61**:1–11.

Bridges AJ, Moos WH, Szotek DL, Trivedi BK, Bristol JA, Heffner TG, Bruns RF, and Downs DA (1987) N6-(2,2-diphenylethyl)adenosine, a novel adenosine receptor agonist with antipsychotic-like activity. *J Med Chem* **30**:1709–1711.

Cerqueira MD (2004) The future of pharmacologic stress: selective A2A adenosine receptor agonists. *Am J Cardiol* **94**: 33D–42D.

Charalambous C, Gsandtner I, Keuerleber S, Milan-Lobo L, Kudlacek O, Freissmuth M, and Zezula J (2008) Restricted collision coupling of the A2A receptor revisited: evidence for physical separation of two signaling cascades. *J Biol Chem* **283**: 9276–9288.

Chen JF, Eltzschig HK, and Fredholm BB (2013) Adenosine receptors as drug targets—what are the challenges? *Nat Rev Drug Discov* **12**:265–286.

Chern Y, Chiou JY, Lai HL, and Tsai MH (1995) Regulation of adenylyl cyclase type VI activity during desensitization of the A2a adenosine receptor-mediated cyclic AMP response: role for protein phosphatase 2A. *Mol Pharmacol* **48**:1–8.

Chern Y, Lai HL, Fong JC, and Liang Y (1993) Multiple mechanisms for desensitization of A2a adenosine receptor-mediated cAMP elevation in rat pheochromocytoma PC12 cells. *Mol Pharmacol* **44**:950–958.

Copeland RA, Pompliano DL, and Meek TD (2006) Drug-target residence time and its implications for lead optimization. *Nat Rev Drug Discov* **5**:730–739.

de Lera Ruiz M, Lim YH, and Zheng J (2014) Adenosine A2A receptor as a drug discovery target. *J Med Chem* **57**:3623–3650.

Deflorian F, Kumar TS, Phan K, Gao ZG, Xu F, Wu H, Katritch V, Stevens RC, and Jacobson KA (2012) Evaluation of molecular modeling of agonist binding in light of the crystallographic structure of an agonist-bound A2A adenosine receptor. *J Med Chem* **55**:538–552.

Ferrandon S, Feinstein TN, Castro M, Wang B, Bouley R, Potts JT, Gardella TJ, and Vilardaga JP (2009) Sustained cyclic AMP production by parathyroid hormone receptor endocytosis. *Nat Chem Biol* **5**:734–742.

Field JJ, Lin G, Okam MM, Majerus E, Keefer J, Onyekwere O, Ross A, Campigotto F, Neuberg D, Linden J, et al. (2013) Sickle cell vaso-occlusion causes activation of iNKT cells that is decreased by the adenosine A2A receptor agonist regadenoson. *Blood* **121**:3329–3334.

Gao ZG and Jacobson KA (2011) Emerging adenosine receptor agonists: an update. *Expert Opin Emerg Drugs* **16**:597–602.

Gnad T, Scheibler S, von Kügelgen I, Scheele C, Kilić A, Glöde A, Hoffmann LS, Reverte-Salisa L, Horn P, Mutlu S, et al. (2014) Adenosine activates brown adipose tissue and recruits beige adipocytes via A2A receptors. *Nature* **516**: 395–399.

Guo D, Hillger JM, IJzerman AP, and Heitman LH (2014) Drug-target residence time—a case for G protein-coupled receptors. *Med Res Rev* **34**:856–892.

Guo D, Mulder-Krieger T, IJzerman AP, and Heitman LH (2012) Functional efficacy of adenosine A2A receptor agonists is positively correlated to their receptor residence time. *Br J Pharmacol* **166**:1846–1859.

Guo D, van Dorp EJ, Mulder-Krieger T, van Veldhoven JP, Brussee J, Ijzerman AP, and Heitman LH (2013) Dual-point competition association assay: a fast and high-throughput kinetic screening method for assessing ligand-receptor binding kinetics. *J Biomol Screen* **18**:309–320.

Haskell-Luevano C, Miwa H, Dickinson C, Hadley ME, Hruby VJ, Yamada T, and Gantz I (1996) Characterizations of the unusual dissociation properties of melanotropin peptides from the melanocortin receptor, hMC1R. *J Med Chem* **39**: 432–435.

Hothersall JD, Bussey CE, Brown AJ, Scott JS, Dale I, and Rawlins P (2015) Sustained wash-resistant receptor activation responses of GPR119 agonists. *Eur J Pharmacol* **762**:430–442.

Hothersall JD, Brown AJ, Dale I, and Rawlins P (2016) Can residence time offer a useful strategy to target agonist drugs for sustained GPCR responses? *Drug Discov Today* **21**:90–96.

Koshiba M, Kojima H, Huang S, Apasov S, and Sitkovsky MV (1997) Memory of extracellular adenosine A2A purinergic receptor-mediated signaling in murine T cells. *J Biol Chem* **272**:25881–25889.

Lebon G, Edwards PC, Leslie AG, and Tate CG (2015) Molecular Determinants of CGS21680 Binding to the Human Adenosine A2A Receptor. *Mol Pharmacol* **87**: 907–915.

Lebon G, Warne T, Edwards PC, Bennett K, Langmead CJ, Leslie AG, and Tate CG (2011) Agonist-bound adenosine A2A receptor structures reveal common features of GPCR activation. *Nature* **474**:521–525.

Lee JY and Lyman E (2012) Agonist dynamics and conformational selection during microsecond simulations of the A(2A) adenosine receptor. *Biophys J* **102**: 2114–2120.

Mantell S, Jones R, and Trevethick M (2010) Design and application of locally delivered agonists of the adenosine A(2A) receptor. *Expert Rev Clin Pharmacol* **3**: 55–72.

Marumoto R, Yoshioka Y, Honjo M, and Kawazoe K (1974), inventors, Takeda Chemical Industries Limited, assignee. 2,6-diaminonebularinderivate 2,6-diaminonebularinderivate. Patent DE2359536 A1. 1973 Nov 29.

Niiya K, Jacobson KA, Silvia SK, and Olsson RA (1993) Covalent binding of a selective agonist irreversibly activates guinea pig coronary artery A2 adenosine receptors. *Naunyn Schmiedebergs Arch Pharmacol* **347**:521–526.

Nishiyama K and Hirai K (2015) In vitro comparison of duration of action of melatonin agonists on melatonin MT receptor: possible link between duration of action and dissociation rate from receptor. *Eur J Pharmacol* **757**:42–52.

Ong S, Liu H, Qiu X, Bhat G, and Pidgeon C (1995) Membrane partition coefficients chromatographically measured using immobilized artificial membrane surfaces. *Anal Chem* **67**:755–762.

Palmer TM, Gettys TW, Jacobson KA, and Stiles GL (1994) Desensitization of the canine A2a adenosine receptor: delineation of multiple processes. *Mol Pharmacol* **45**:1082–1094.

Palmgren JJ, Monkkonen J, Korjamo T, Hassinen A, and Auriola S (2006) Drug adsorption to plastic containers and retention of drugs in cultured cells under in vitro conditions. *Eur J Pharm Biopharm* **64**: 369–378.

Pidgeon C, Ong S, Liu H, Qiu X, Pidgeon M, Dantzig AH, Munroe J, Hornback WJ, Kasher JS, Glunz L, et al. (1995) IAM chromatography: an in vitro screen for predicting drug membrane permeability. *J Med Chem* **38**:590–594.

Sato N, Yuki Y, Shinohara H, Takeji Y, Ito K, Michikami D, Hino K, and Yamazaki H (2010) inventors, Otsuka Pharmaceutical Co Ltd, assignee. A novel cyanopyrimidine derivative. Patent WO/2010/090299. 2010 Dec 8.

Sykes DA, Parry C, Reilly J, Wright P, Fairhurst RA, and Charlton SJ (2014) Observed drug-receptor association rates are governed by membrane affinity: the

importance of establishing "micro-pharmacokinetic/pharmacodynamic relationships" at the β2-adrenoceptor. *Mol Pharmacol* **85**:608–617.

Teschemacher A and Lemoine H (1999) Kinetic analysis of drug-receptor interactions of long-acting beta2 sympathomimetics in isolated receptor membranes: evidence against prolonged effects of salmeterol and formoterol on receptor-coupled adenylyl cyclase. *J Pharmacol Exp Ther* **288**:1084–1092.

Vauquelin G and Charlton SJ (2010) Long-lasting target binding and rebinding as mechanisms to prolong in vivo drug action. *Br J Pharmacol* **161**:488–508.

Wennerberg M, Balendran A, Clapham JC, and Vauquelin G (2010) Unravelling the complex dissociation of [(3)H]-rimonabant from plated CB(1) cannabinoid receptor-expressing cells. *Fundam Clin Pharmacol* **24**:181–187.

Xu F, Wu H, Katritch V, Han GW, Jacobson KA, Gao ZG, Cherezov V, and Stevens RC (2011) Structure of an agonist-bound human A2A adenosine receptor. *Science* **332**:322–327.

Zezula J and Freissmuth M (2008) The A(2A)-adenosine receptor: a GPCR with unique features? *Br J Pharmacol* **153** (Suppl 1):S184–S190.

Address correspondence to: Philip Rawlins, AstraZeneca, Discovery Sciences, Unit 310 – Darwin Building, Cambridge Science Park, Milton Road, Cambridge, CB4 0WG. E-mail: philip.rawlins@astrazeneca.com
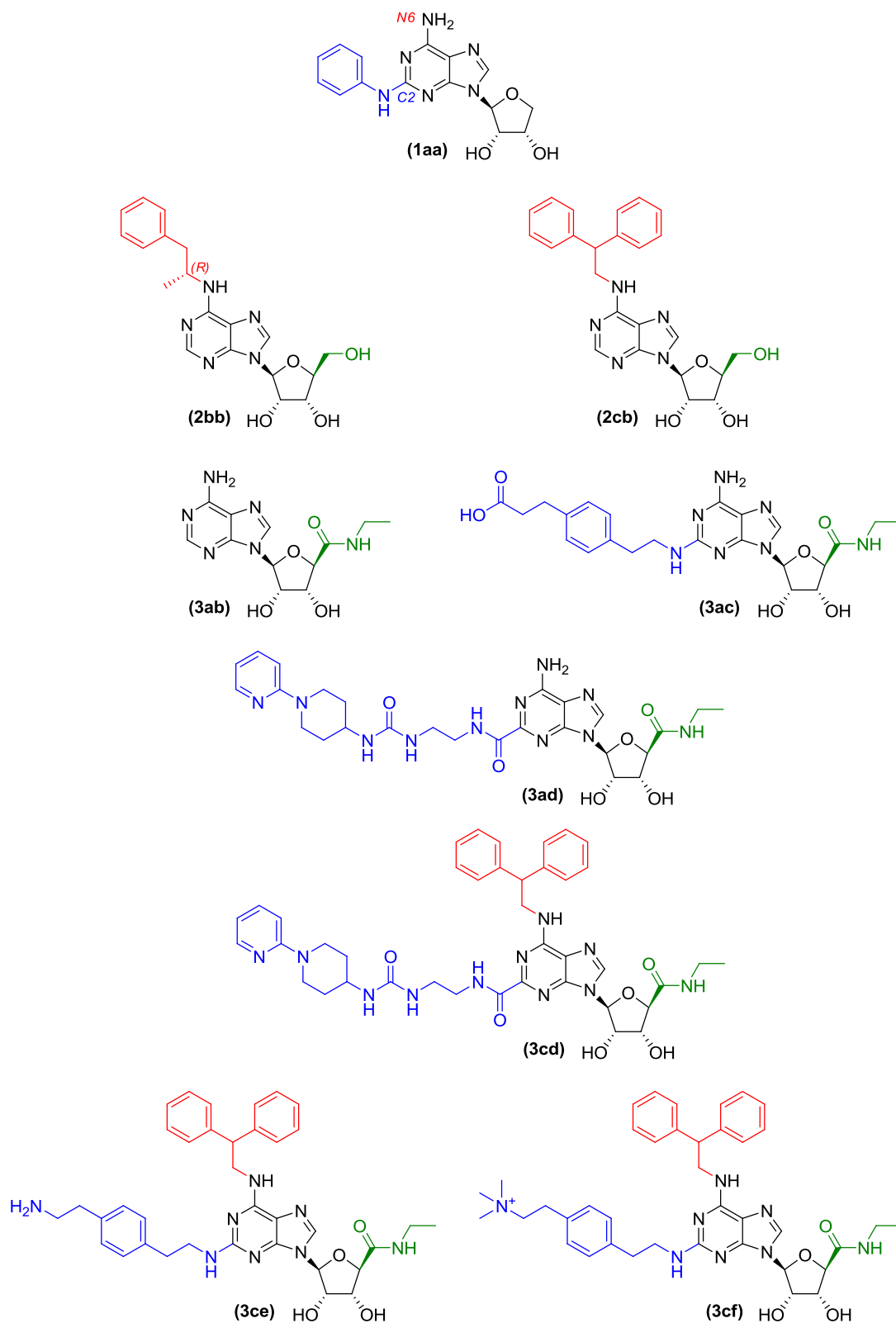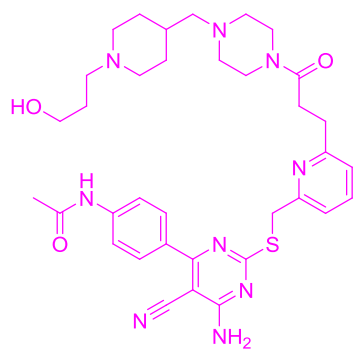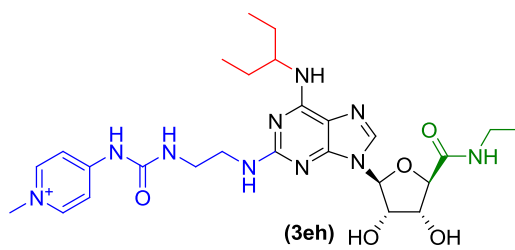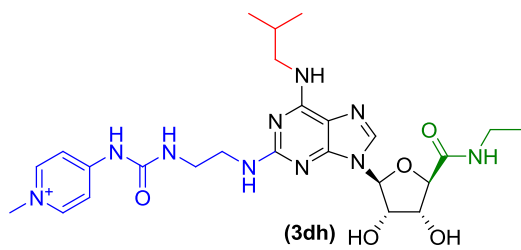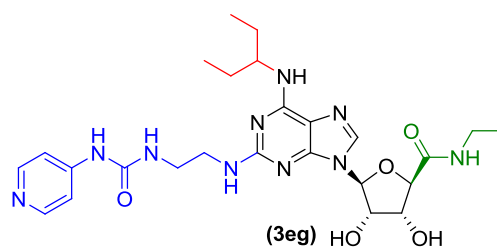
Supplemental Data:

**"Structure activity relationships of the sustained effects of adenosine A2A receptor agonists driven by slow dissociation kinetics"**

J. Daniel Hothersall, Dong Guo, Sunil Sarda, Robert J. Sheppard, Hongming Chen, Wesley Keur, Michael J. Waring, Adriaan P. IJzerman, Stephen J. Hill, Ian L. Dale, Philip B. Rawlins

**Supplemental Figure 1.** The structures of the ligands investigated in this study. All the ligands have an adenosine scaffold (black), with substitution on the ribose 4 position (R1 green), N6 (R2; red), and/or C2 (R3; blue). Compound 4 is shown in magenta as it does not share this structural scaffold.

(3ag)

(3cg)

(3dg)

(3eg)

(3ah)

(3ch)

(3dh)

(3eh)

(4)
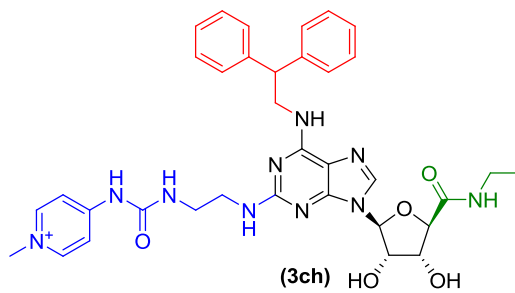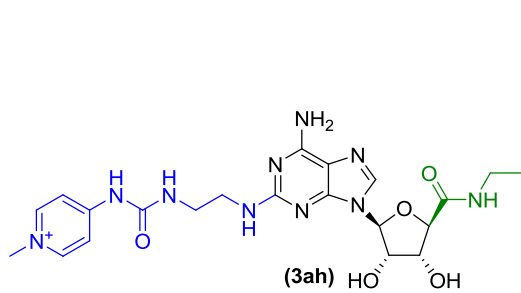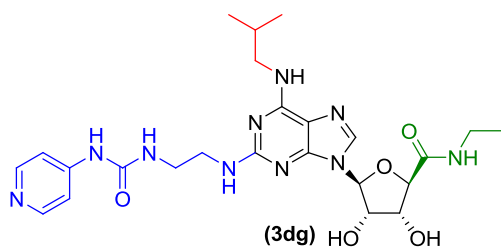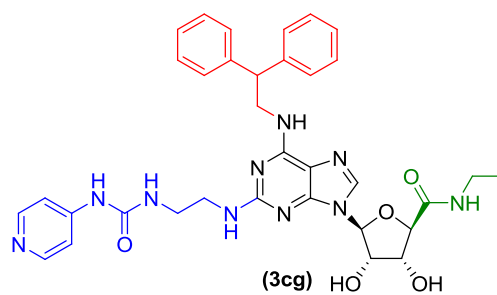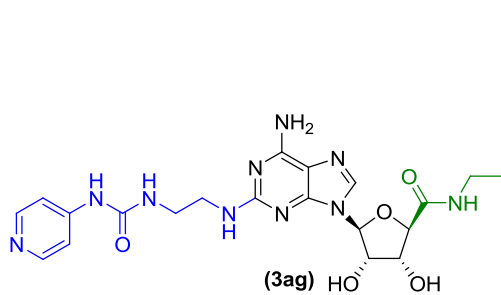
Supplemental Figure 2. Example concentration-response curves measured using the GloSensor cAMP assay in CHO-A2A cells (100 minutes, 20 °C) for the A2A agonists 3ab (dark blue), 3ac (light blue), 3cd (light green), 1aa (light purple), 3ch (red), 3eg (yellow), 3ad (dark red), and 4 (dark purple). Data represent the average of three experiments performed in triplicate, and derived pEC50 values are shown in Table 2 of main text.
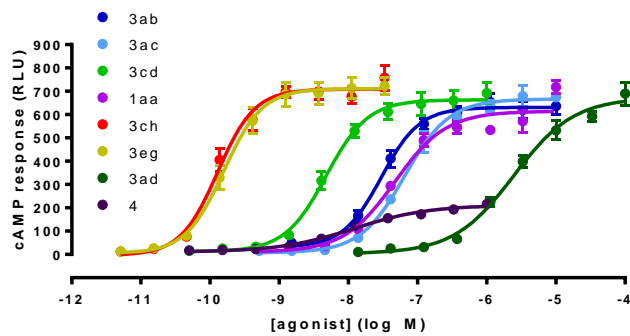
S u p p l e m e n t a l   F i g u r e   2

Supplemental Figure 3. Control experiments verifying the GloSensor reversal assay to estimate agonist off-rate. **(A-B)** GloSensor traces (20 °C) demonstrating competitive antagonism of 3cd (A) or 3ch (B) agonist responses by ZM-241385. Cells were incubated with (red) or without (blue) 100 nM ZM-241385 for 100 minutes before direct addition of supramaximal concentrations (100 x EC_{50}) of each agonist and further incubation for 200 minutes. Pre-equilibration with antagonist prevents agonist cAMP responses, indicating competitive antagonism. Data represent an average of three experiments performed in triplicate. **(C-D)** For comparison in a separate assay format, reversal traces were also measured in the endpoint HTRF cAMP assay, with no PDE inclusion to measure dynamic changes in cellular cAMP. (C) Cells were incubated with EC_{90} concentrations of 3cd, 1aa, 3ch, 3dh, 3eg, 3ce, or 3cf for 2 hours at room temperature before direct addition of vehicle control of excess antagonist (100 nM ZM-241385) and incubation for a range of times up to 300 minutes at room temperature before cells were lysed and cAMP measured. Reversal responses with antagonist treatment were normalized to vehicle at each time-point and traces fitted to non-linear regression (one-phase exponential decay). Data represent an average of three experiments performed in triplicate. (D) Derived t½ values from the HTRF assay shown in (C) were plotted against those derived in the GloSensor assay (Table 2 in main text) and linear regression performed. There was a strong correlation between the two data sets ($r^2 = 1.00$, $P < 0.0001$, n = 7 ligands) indicating that the GloSensor assay accurately reflects cellular cAMP fluxes.

A

± ZM-241385

+ compound 3cd

cAMP response (RLU)

- vehlicle
- ZM-241385

time (min)

B

± ZM-241385

+ compund 3ch

cAMP response (RLU)

- vehicle
- ZM-241385

time (min)

C

endpoint cAMP assay reversal

cAMP response (% vehicle)

- 3cd
- 1aa
- 3ch
- 3dh
- 3eg
- 3ce
- 3cf

time (min)

D

GloSensor (t $_{1/2}$ min)

$r^2 = 1.00$, P < 0.0001

HTRF (t $_{1/2}$ min)
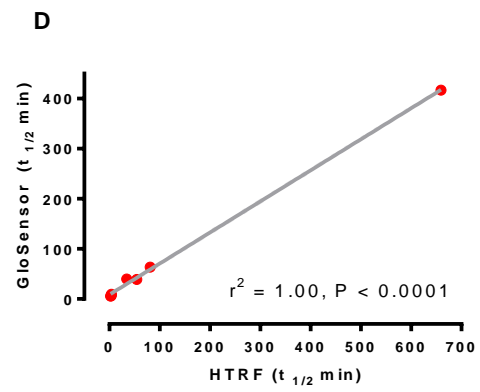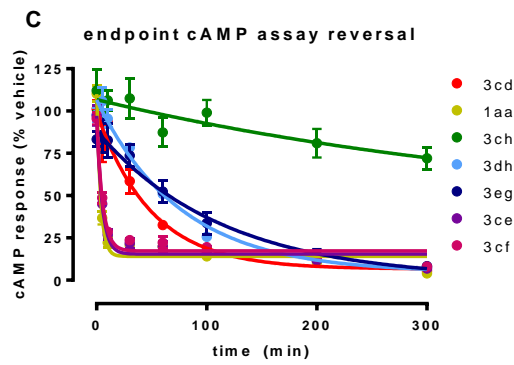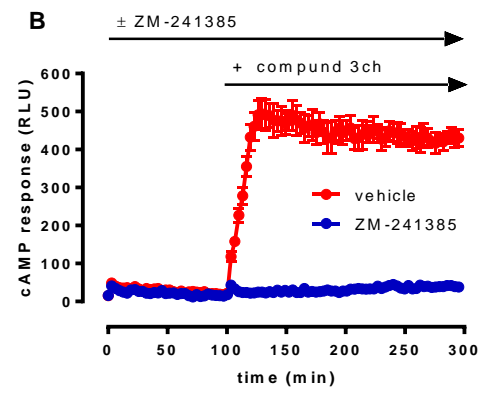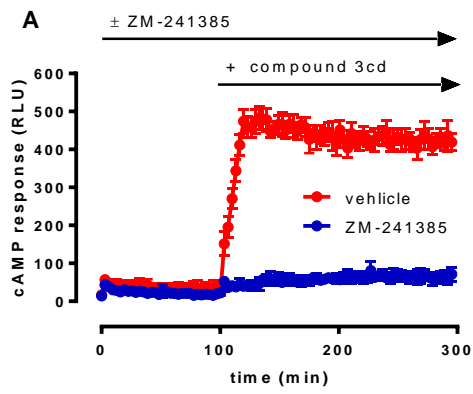
Supplemental Figure 3

Supplemental Figure 4. Compound 3ce is unique amongst the ligands tested in its ability to discriminate between antagonists in reversal experiments as it appears rapidly reversed when ZM-241385 is applied, but slowly/incompletely reversed when LUF5834 is applied. Thus, applying LUF5834 reversal data confirms that 3ce is a sustained wash-resistant agonist with a slow off-rate, thus explaining the anomaly highlighted in Figure 3H for this compound. **(A-C)** GloSensor antagonist reversal traces observed when ZM-241385 (blue; 100 nM) or LUF5834 (red; 6 μM) is added after generation of stable agonist responses. 3ce (A) is rapidly and completely reversed by ZM-241385 but only partially reversed by LUF5834. For comparison, 1aa (B) is rapidly reversed in a very similar manner by both antagonists, whilst 3ch (C) is poorly reversed by both. **(D)** GloSensor agonist stimulation responses of 3cd (red) and LUF5834 (blue) to demonstrate that LUF5834 has very weak efficacy in this system at a saturating concentration. **(E)** Comparison of reversal rates (t½) derived from GloSensor experiments using ZM-241385 (100 nM) and LUF5834 (6 μM) as reversal agents show strong correlation across 18 agonists tested, although 3ce (highlighted as a red circle) is a clear outlier. Linear regression analysis displayed an r^2 of 0.95 and P < 0.001. Therefore, with 3ce as an exception, consistent kinetic data was obtained regardless of the antagonist used, suggesting that derived reversal rates were not an artefact of the pharmacology of ZM-241385. All GloSensor traces represent an average of three experiments performed in triplicate.

A compound 3ce

**B** compound 1aa

C compound 3ch

D

E comparaitve reversal rates
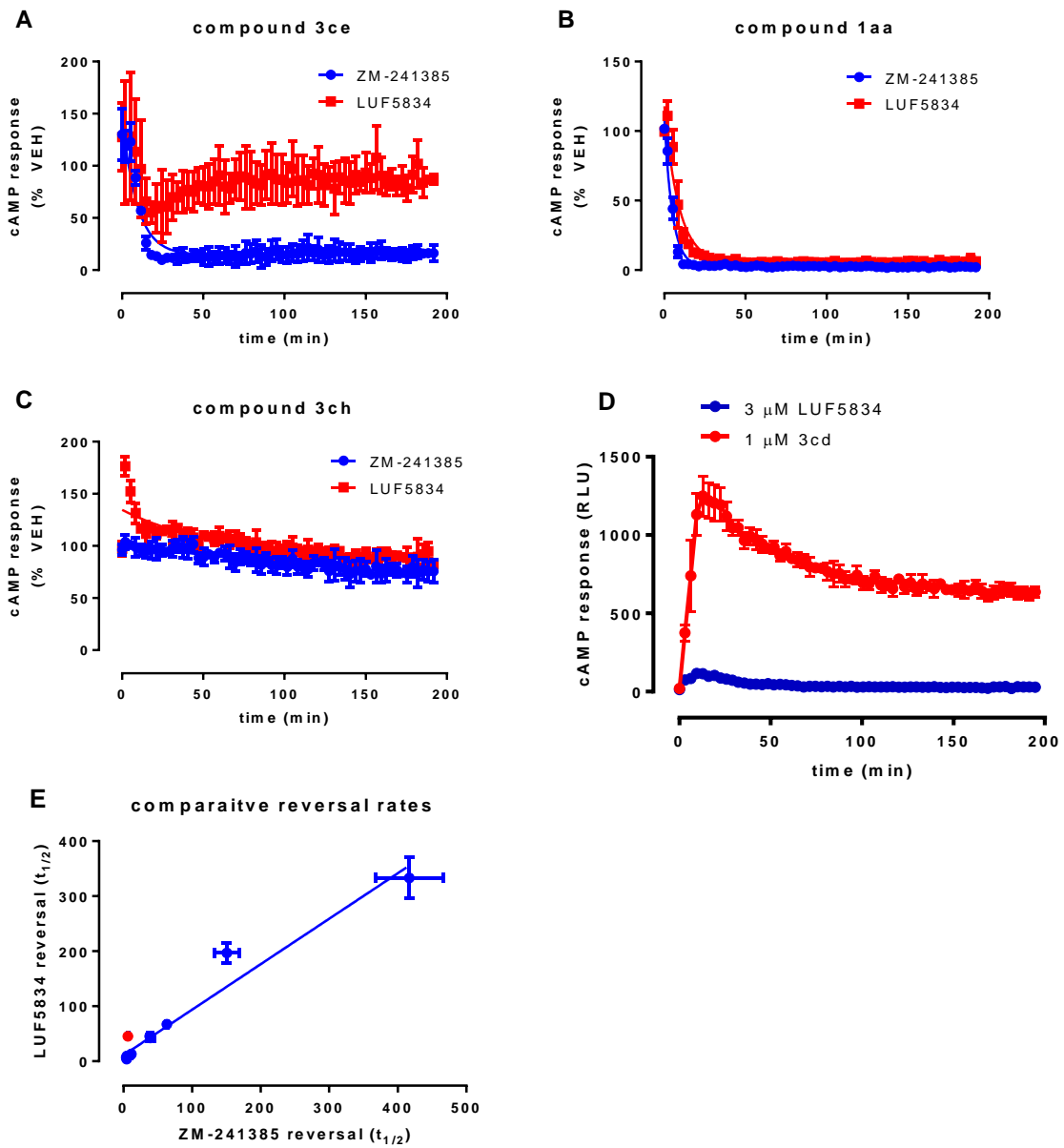
S u p p l e m e n t a l   F i g u r e   4

Supplemental Figure 5. Control experiments supporting [^{3}H]ZM-241385 binding data. **(A)** [^{3}H]ZM-241385 association binding rate at 4 °C under control conditions (black) or in the presence of Ki concentrations of test compound. **(B)** Best-fit data derived from these curves is shown as a table. **(C-E)** Antagonist reversal of A2A agonist responses in membranes prepared from CHO-A2A cells. These experiments used the HTRF HiRange cAMP kit (CisBio). Methods to prepare membranes were based on those described previously (Palmer et al., 1994). Cells were grown to confluency in two 225 cm^2 flasks and washed twice with ice-cold PBS. Cells were then lysed and scraped in ice-cold lysis buffer (50 mM TRIS, 5 mM EDTA, pH 7.4), followed by incubation at 4 °C for 10 minutes. Cell lysates were homogenized using a glass-on-glass Dounce homogenizer, and then centrifuged at 42,000 x g for 15 minutes at 4 °C. The sample was then washed once with assay buffer (50 mM TRIS, pH 7.4) without disturbing the pellet, and then resuspended in 20 ml of assay buffer using the homogenizer and by passing through a fine needle. Membranes were prepared fresh immediately prior to each experiment. The membrane suspension was then supplemented with 5 mM MgCl$_2$ and 0.8 U/ml adenosine deaminase and 50 μl/well added to 96 well plates. 10 x concentrated agonist (final concentration EC$_{90}$) was then directly added and the plates incubated at room temperature for 2 hours. Antagonist (100 nM ZM-241385) was then directly added to these wells and incubated for a further 0, 1, 2, or 3 hours at room temperature. cAMP was then captured by direct addition of stimulation buffer in a 1:1 dilution to achieve final concentrations of 40 μM rolipram, 1 mM ATP, 5 mM MgCl$_2$, and 0.8 U/ml adenosine deaminase, and membranes incubated for a further 45 minutes at room temperature, before 10 μl of sample was added to a 384 well plate to measure cAMP levels by HTRF assay as per the manufacturer's instructions. In these experiments, A2A cAMP responses remained stable over time. The antagonist reversed 1aa (C) responses to near baseline within the first hour (this is likely a gross underestimation of reversal rate) with significantly reduced responses compared to vehicle (P < 0.001; ANOVA: n = 3). In marked contrast, whilst the antagonist reversed 3cd-mediated (D) cAMP responses to significantly decreased levels after 2 hours (P < 0.05; ANOVA: n = 3), this reversal was incomplete and reached only 79.56 ± 8.46 % of vehicle. 3ch (E) responses were not significantly affected by antagonist. Therefore, the slow off-rates of 3cd and 3ch are maintained in cAMP reversal responses in membranes, and the 3cd responses are more poorly reversed than in cells. Therefore, the

use of membranes, different cell background or non-equivalent buffer system compared to radioligand binding did not influence our findings.

A
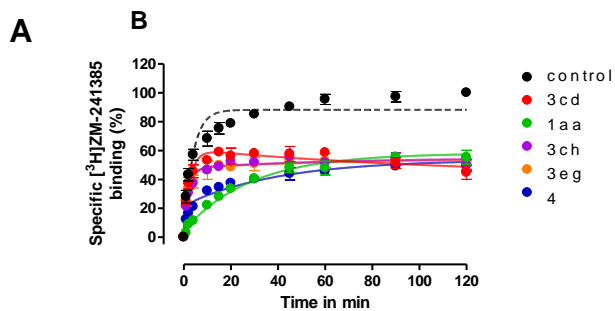
B

Compound	Affinity, K_i (nM)	k_{on} ($M^{-1} \cdot min^{-1}$)	k_{off} (min^{-1})	RT (min)
3cd	44 ± 5	$3.5 \pm 0.4 \times 10^5$	0.0057 ± 0.0024	175 ± 74
1aa	154 ± 31	$3.3 \pm 2.0 \times 10^6$	0.41 ± 0.26	2.4 ± 1.5
3ch	15 ± 2	$1.8 \pm 0.2 \times 10^6$	0.019 ± 0.005	53 ± 14
3eg	66 ± 11	$4.7 \pm 0.6 \times 10^5$	0.018 ± 0.005	56 ± 16
4	24 ± 1	$4.7 \pm 0.9 \times 10^6$	0.059 ± 0.014	17 ± 4

C

D

E
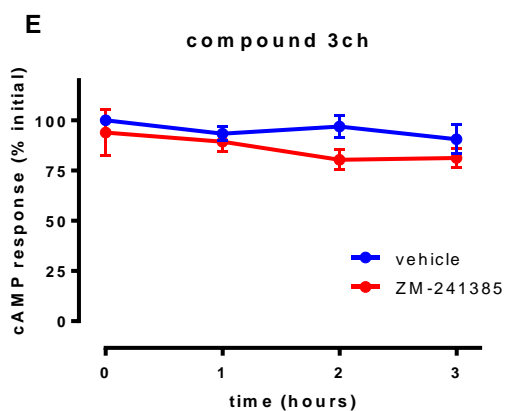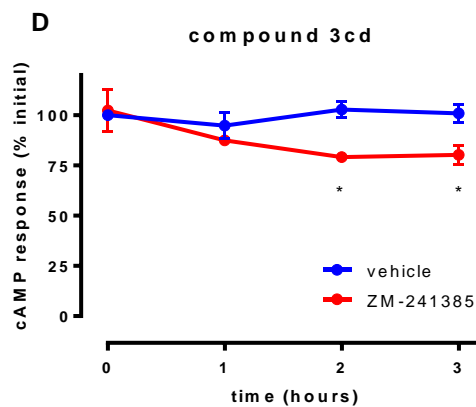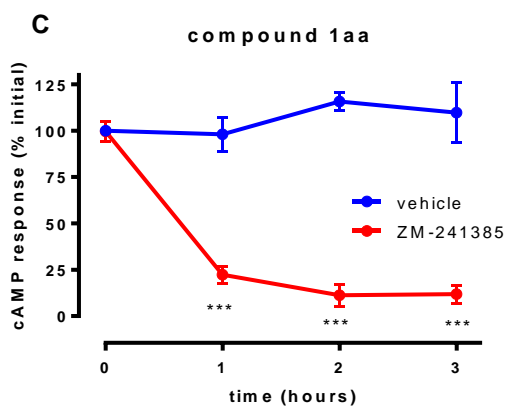
Supplemental Figure 5

Supplemental Figure 6. Concentration-response curves of agonists in CHO-A2B cells measured using the endpoint cAMP assay. 3ab (red), 3cd (green), 3ch (blue) or 3eg (purple) were incubated for 45 minutes at 37 °C with 40 μM rolipram before cAMP measured by HTRF. All agonists show robust and saturable A2B responses with response maxima comparable to 3ab.
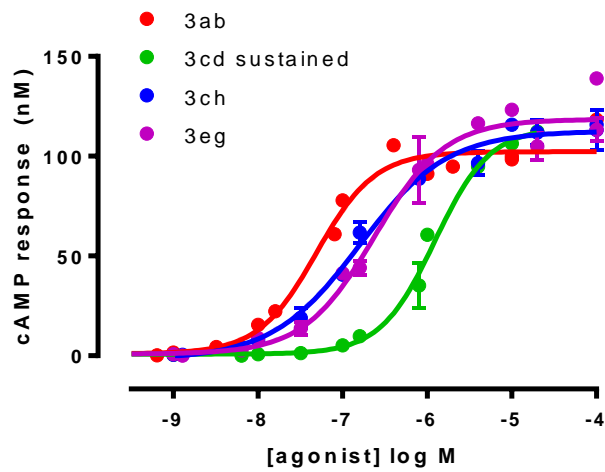
S u p p l e m e n t a l   F i g u r e   6

Supplemental Figure 7. Concentration-response curves of A2A agonists in SH-SY5Y cells measured using the endpoint cAMP assay. To confirm receptor-specificity, cells were pre-treated with the A2A-selective antagonist SCH-442416 (100 nM) (red) or vehicle control (blue) for 30 minutes (37 °C) before addition of either 3cd (A), 1aa (B), or 3ch (C) for a further 45 minutes (37 °C) in the presence of 40 μM rolipram, and subsequent measurement of cAMP by HTRF. Derived pEC50 values are 8.59 ± 0.09, 7.00 ± 0.23, and 8.90 ± 0.05 for these agonists, respectively, consistent with their A2A-activity. Moreover, the antagonist caused a right-ward shift in the curves with dose ratios of > 15, supporting a role for A2A responses. Together, these findings suggest that the cAMP responses evoked by these ligands are at least predominantly A2A-mediated.
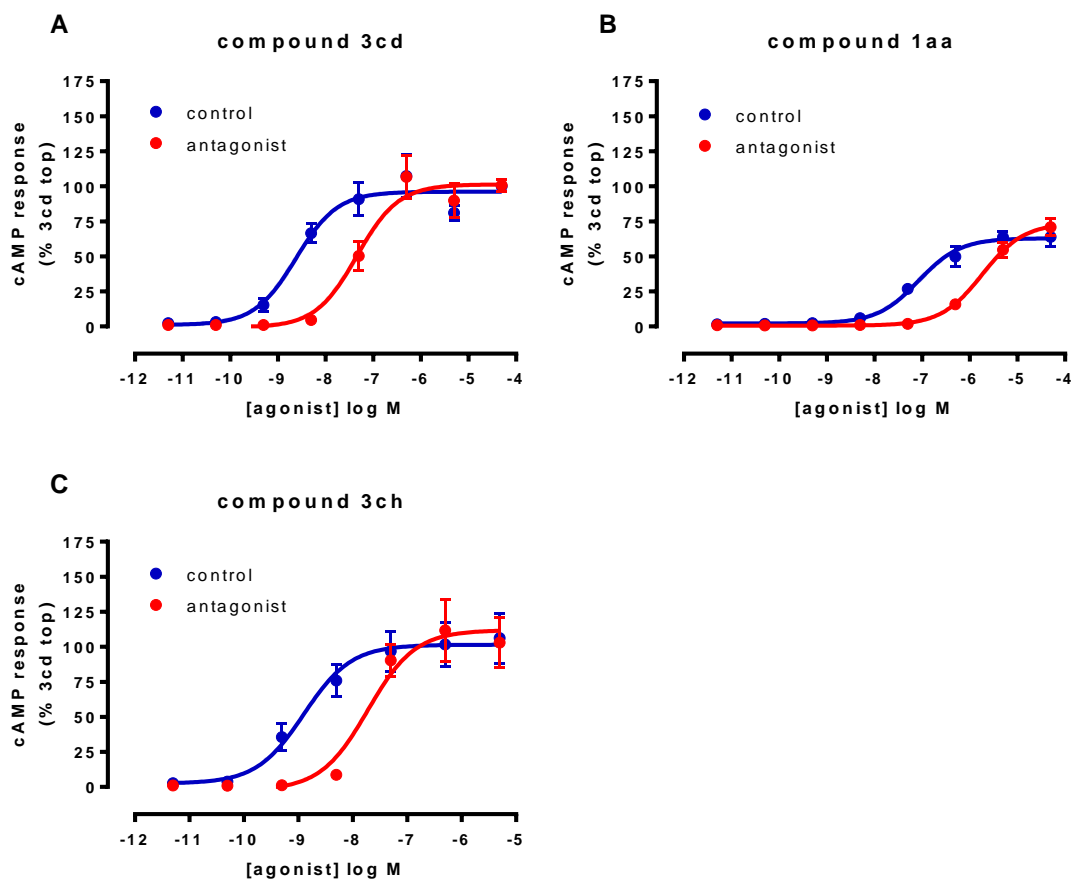
Supplemental Figure 7

Supplemental Schemes:
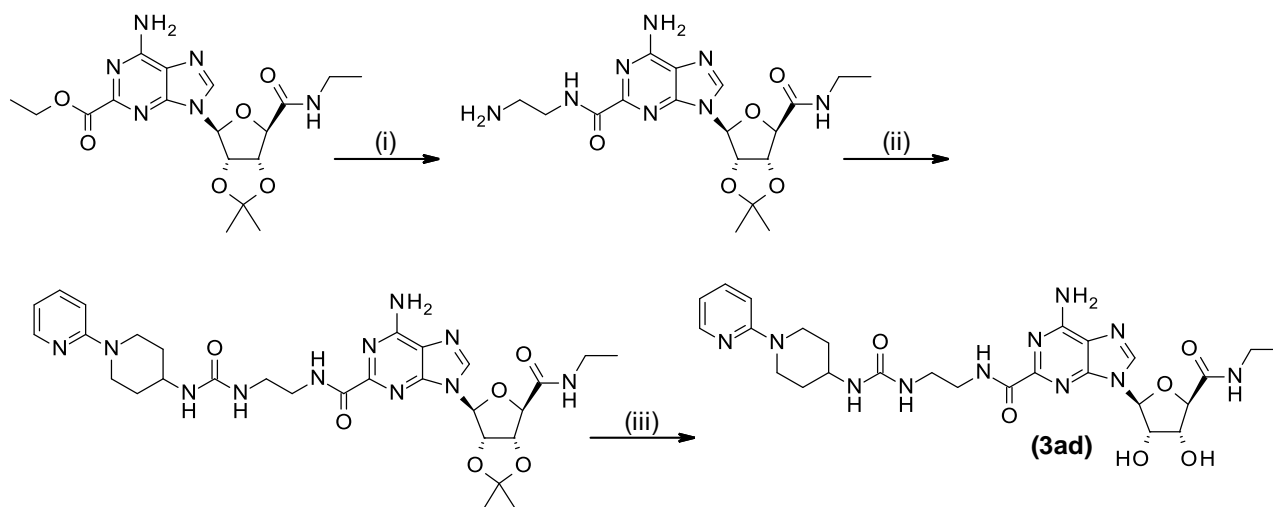
Supplemental Scheme 1: (i) ethane-1,2-diamine, acetone, 80°C, 3 h, 52%; (ii) *N*-(1-(pyridin-2-yl)piperidin-4-yl)-1*H*-imidazole-1-carboxamide, iPrOH, toluene, DCM, 24 h; (iii) HCl (1 M), 65°C, 1 h, 39% (over 2 steps).

6-amino-*N*-(2-aminoethyl)-9-((3a*S*,4*S*,6*R*,6a*R*)-6-(ethylcarbamoyl)-2,2-dimethyltetrahydrofuro[3,4-*d*][1,3]dioxol-4-yl)-9*H*-purine-2-carboxamide

A stirred mixture of ethyl 6-amino-9-((3a*S*,4*S*,6*R*,6a*R*)-6-(ethylcarbamoyl)-2,2-dimethyltetrahydrofuro[3,4-*d*][1,3]dioxol-4-yl)-9*H*-purine-2-carboxylate (0.500 g, 1.19 mmol) and etane-1,2-diamine (5 mL, 75 mmol) was heated to 80°C for 3 h. After cooling, the mixture was concentrated *in vacuo* and purified by preparative HPLC to give 6-amino-*N*-(2-aminoethyl)-9-((3a*S*,4*S*,6*R*,6a*R*)-6-(ethylcarbamoyl)-2,2-dimethyltetrahydrofuro[3,4-*d*][1,3]dioxol-4-yl)-9*H*-purine-2-carboxamide (0.268 g, 0.62 mmol, 52%).

6-amino-9-((3a*S*,4*S*,6*R*,6a*R*)-6-(ethylcarbamoyl)-2,2-dimethyltetrahydrofuro[3,4-*d*][1,3]dioxol-4-yl)-*N*-(2-(3-(1-(pyridin-2-yl)piperidin-4-yl)ureido)ethyl)-9*H*-purine-2-carboxamide

A stirred solution of 6-amino-*N*-(2-aminoethyl)-9-((3a*S*,4*S*,6*R*,6a*R*)-6-(ethylcarbamoyl)-2,2-dimethyltetrahydrofuro[3,4-*d*][1,3]dioxol-4-yl)-9*H*-purine-2-carboxamide (0.079 g, 0.18 mmol) in toluene (4 mL) and iPrOH (1 mL) was treated with a solution of *N*-(1-(pyridin-2-yl)piperidin-4-yl)-1*H*-imidazole-1-carboxamide (0.049 g, 0.18 mmol) in DCM (2.5 mL). The mixture was stirred at

room tempertautre for 24 h then concentrated *in vacuo* to give a residue containing 6-amino-9-((3a*S*,4*S*,6*R*,6a*R*)-6-(ethylcarbamoyl)-2,2-dimethyltetrahydrofuro[3,4-*d*][1,3]dioxol-4-yl)-*N*-(2-(3-(1-(pyridin-2-yl)piperidin-4-yl)ureido)ethyl)-9*H*-purine-2-carboxamide, which was taken on to the next step without purification.

6-amino-9-((2*S*,3*S*,4*R*,5*R*)-5-(ethylcarbamoyl)-3,4-dihydroxytetrahydrofuran-2-yl)-*N*-(2-(3-(1-(pyridin-2-yl)piperidin-4-yl)ureido)ethyl)-9*H*-purine-2-carboxamide

A residue containing 6-amino-9-((3a*S*,4*S*,6*R*,6a*R*)-6-(ethylcarbamoyl)-2,2-dimethyltetrahydrofuro[3,4-*d*][1,3]dioxol-4-yl)-*N*-(2-(3-(1-(pyridin-2-yl)piperidin-4-yl)ureido)ethyl)-9*H*-purine-2-carboxamide (0.18 mmol) was treated with HCl (1 M) (1.5 mL) and heated at 65°C. After stirring for 1 h the mixture was concentrated *in vacuo* and purified by preparative HPLC to give 6-amino-9-((2*S*,3*S*,4*R*,5*R*)-5-(ethylcarbamoyl)-3,4-dihydroxytetrahydrofuran-2-yl)-*N*-(2-(3-(1-(pyridin-2-yl)piperidin-4-yl)ureido)ethyl)-9*H*-purine-2-carboxamide (0.042 g, 0.070 mmol, 39% over two steps).
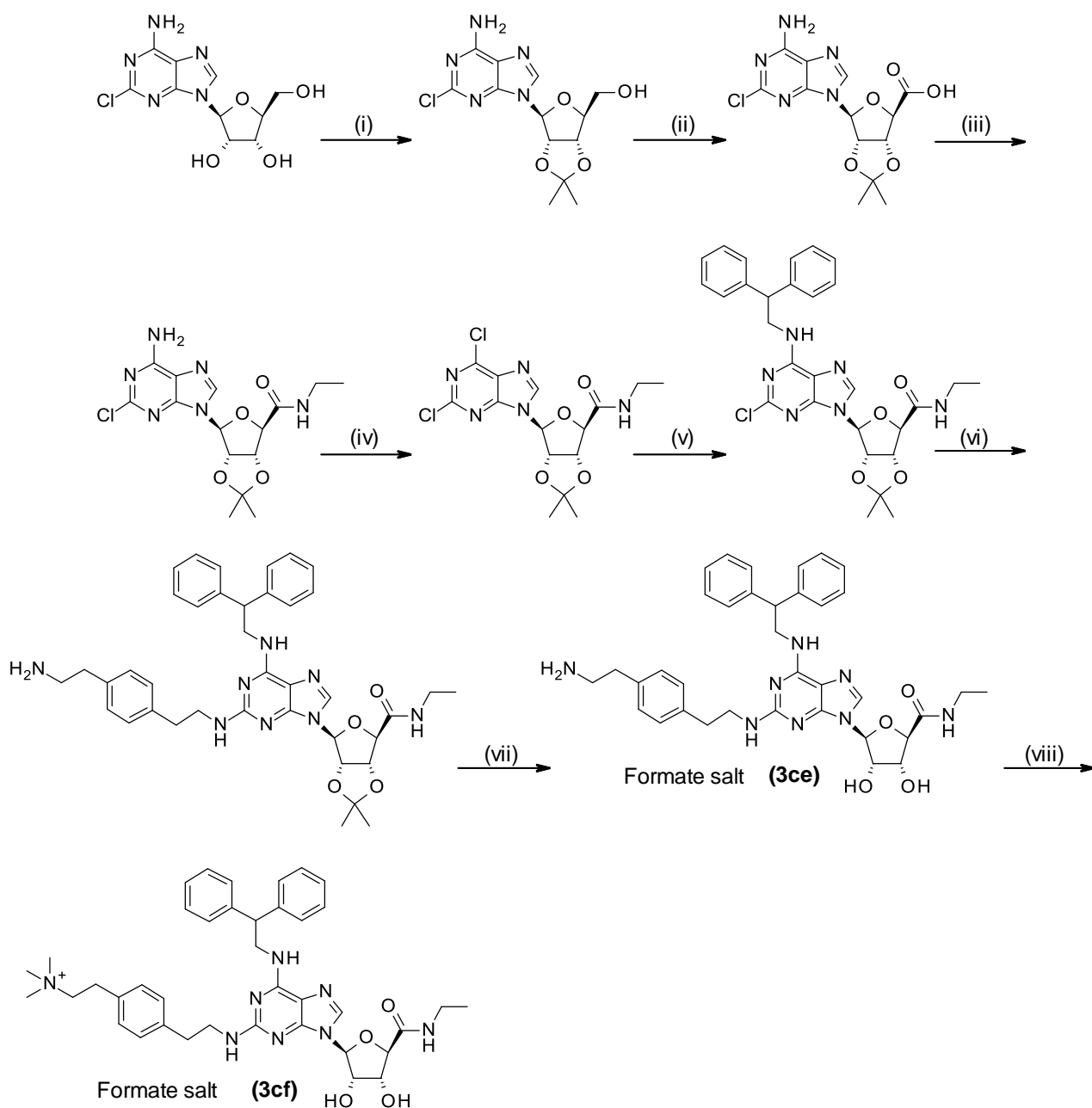
Supplemental Scheme 2: (i) 2,2-dimethoxypropane, TsOH.H_2O, acetone, r.t., 20 h, 88%; (ii)

KMnO$_4$, KOH, MeCN, H_2O, r.t., 20 h, then H_2O_2 (30%), followed by HCl (2 M), 73%; (iii) Thionyl

chloride, DCM, DMF (cat.) 50°C, 4 h, then ethylamine, DCM, 0-5°C, 2 h, 74%; (iv) *t*-Butyl nitrite,

CCl$_4$, MeCN, 80°C, 4 h, 30%; (v) 2,2-diphenylethanamine, EtOH, r.t., 20 h, 94%; (vi) 2,2'-(1,4-

phenylene)diethanamine, 130°C, 2 h, 67%; (vii) HCl (1 M), 60°C, 1 h, 50%; (viii) Iodomethane,

K$_2$CO$_3$, MeOH, 30°C, 7 h, 47%.

((3a*S*,4*S*,6*S*,6a*S*)-6-(6-amino-2-chloro-9*H*-purin-9-yl)-2,2-dimethyltetrahydrofuro[3,4-*d*][1,3]dioxol-4-yl)methanol

A stirred mixture of (2*S*,3*S*,4*R*,5*S*)-2-(6-amino-2-chloro-9*H*-purin-9-yl)-5-(hydroxymethyl)tetrahydrofuran-3,4-diol (50 g, 166 mmol), *p*-toluenesulfonic acid monohydrate (31.45 g, 166 mmol), 2,2-dimethoxypropane (357 mL, 2903 mmol), and acetone (690 mL) was stirred at room temperature. After 20 h water (400 mL) was added and the mixture adjusted to pH =7-8 by the addition of ammonia solution. The solvent was removed *in vacuo*, and the residue partitioned between EtOAc and water. The organic extracts were concentrated *in vacuo* to give ((3a*S*,4*S*,6*S*,6a*S*)-6-(6-amino-2-chloro-9*H*-purin-9-yl)-2,2-dimethyltetrahydrofuro[3,4-*d*][1,3]dioxol-4-yl)methanol (50 g, 146 mmol, 88%) as a white solid.

(3a*R*,4*R*,6*S*,6a*S*)-6-(6-amino-2-chloro-9*H*-purin-9-yl)-2,2-dimethyltetrahydrofuro[3,4-*d*][1,3]dioxole-4-carboxylic acid

A stirred mixture of ((3a*S*,4*S*,6*S*,6a*S*)-6-(6-amino-2-chloro-9*H*-purin-9-yl)-2,2-dimethyltetrahydrofuro[3,4-*d*][1,3]dioxol-4-yl)methanol (50 g, 146 mmol) and potassium hydroxide (24.6 g, 439 mmol) in water/MeCN (400 mL/1600 ml) was treated with a solution of KMnO$_4$ (69.3 g, 439 mmol) in water (720 mL). The resulting mixture was stirred at room temperature for 20 h, then filtered through Celite. Hydrogen peroxide (30%) (100 mL) was added to the filtrate. The organic solvent was removed *in vacuo*, and the remaining aqueous adjusted to pH = 4 by the addition of HCl (1 M). The resulting precipitate was removed by filtration and dried *in vacuo* to afford (3a*R*,4*R*,6*S*,6a*S*)-6-(6-amino-2-chloro-9*H*-purin-9-yl)-2,2-dimethyltetrahydrofuro[3,4-*d*][1,3]dioxole-4-carboxylic acid (38 g, 107 mmol, 73%) as a white solid.

(3a*R*,4*R*,6*S*,6a*S*)-6-(6-amino-2-chloro-9*H*-purin-9-yl)-*N*-ethyl-2,2-dimethyltetrahydrofuro[3,4-*d*][1,3]dioxole-4-carboxamide

A stirred mixture of (3a*R*,4*R*,6*S*,6a*S*)-6-(6-amino-2-chloro-9*H*-purin-9-yl)-2,2-dimethyltetrahydrofuro[3,4-*d*][1,3]dioxole-4-carboxylic acid (15 g, 42 mmol), DMF (0.6 mL) and thionyl chloride (75 mL, 1034 mmol) was heated to 50°C for 4 h, then the solvent was removed *in vacuo*. The residue was suspended in DCM (240 mL), and then added in portions to a solution of

ethylamine (65-70% solution in H₂O) (48 mL) dissolved in DCM (200 mL) at 0-5°C. After stirring

for 2 h the mixture was poured onto water. The organic layer was dried (Na₂SO₄), filtered, and

concentrated *in vacuo* to give (3a*R*,4*R*,6*S*,6a*S*)-6-(6-amino-2-chloro-9*H*-purin-9-yl)-*N*-ethyl-2,2-

dimethyltetrahydrofuro[3,4-*d*][1,3]dioxole-4-carboxamide (12 g, 31 mmol, 74%) as a white solid.

(3a*R*,4*R*,6*S*,6a*S*)-6-(2,6-dichloro-9*H*-purin-9-yl)-*N*-ethyl-2,2-dimethyltetrahydrofuro[3,4-
***d*][1,3]dioxole-4-carboxamide**

A stirred mixture of (3a*R*,4*R*,6*S*,6a*S*)-6-(6-amino-2-chloro-9*H*-purin-9-yl)-*N*-ethyl-2,2-

dimethyltetrahydrofuro[3,4-*d*][1,3]dioxole-4-carboxamide (10 g, 26 mmol) and carbon tetrachloride

(270 mL) in acetonitrile (67 mL) was treated with *tert*-butyl nitrite (9.31 mL, 78 mmol). The mixture

was stirred for 4 h at 80°C, then concentrated *in vacuo*. The residue was purified by flash

chromatography (silica), eluting with methanol in DCM (2%), to give (3a*R*,4*R*,6*S*,6a*S*)-6-(2,6-

dichloro-9*H*-purin-9-yl)-*N*-ethyl-2,2-dimethyltetrahydrofuro[3,4-d][1,3]dioxole-4-carboxamide (3.2 g,

7.96 mmol, 30%) as a yellow solid.

(3a*R*,4*R*,6*S*,6a*S*)-6-(2-chloro-6-(2,2-diphenylethylamino)-9*H*-purin-9-yl)-*N*-ethyl-2,2-
dimethyltetrahydrofuro[3,4-*d*][1,3]dioxole-4-carboxamide

To a stirred solution of (3a*R*,4*R*,6*S*,6a*S*)-6-(2,6-dichloro-9*H*-purin-9-yl)-*N*-ethyl-2,2-

dimethyltetrahydrofuro[3,4-*d*][1,3]dioxole-4-carboxamide (1.6 g, 4.0 mmol) in ethanol (40 mL) was

added 2,2-diphenylethylamine (7.8 g, 39 mmol). The mixture was stirred at room temperature for 20

h then concentrated *in vacuo*. The resulting residue was dissolved in EtOAc and washed with HCl (2

M) (50 mL). The organic layer was dried (Na₂SO₄), filtered, and concentrated *in vacuo* to give a

residue which was purified by flash chromatography (silica), eluting with methanol in DCM (2%), to

afford (3a*R*,4*R*,6*S*,6a*S*)-6-(2-chloro-6-(2,2-diphenylethylamino)-9*H*-purin-9-yl)-*N*-ethyl-2,2-

dimethyltetrahydrofuro[3,4-*d*][1,3]dioxole-4-carboxamide (2.1 g, 3.7 mmol, 94%) as a yellow solid.

(3a*R*,4*R*,6*S*,6a*S*)-6-(2-(4-(2-aminoethyl)phenethylamino)-6-(2,2-diphenylethylamino)-9*H*-purin-
9-yl)-*N*-ethyl-2,2-dimethyltetrahydrofuro[3,4-*d*][1,3]dioxole-4-carboxamide

A stirred mixture of (3a*R*,4*R*,6*S*,6a*S*)-6-(2-chloro-6-(2,2-diphenylethylamino)-9*H*-purin-9-yl)-*N*-ethyl-2,2-dimethyltetrahydrofuro[3,4-*d*][1,3]dioxole-4-carboxamide (0.489 g, 0.87 mmol) and 2,2'-(1,4-phenylene)diethanamine (1.0 g, 6.1 mmol) was heated to 130°C. After 2 h the mixture was allowed to cool, then purified by flash chromatography (silica), eluting with methanol in DCM (16%), to afford (3a*R*,4*R*,6*S*,6a*S*)-6-(2-(4-(2-aminoethyl)phenethylamino)-6-(2,2-diphenylethylamino)-9*H*-purin-9-yl)-*N*-ethyl-2,2-dimethyltetrahydrofuro[3,4-*d*][1,3]dioxole-4-carboxamide (0.400 g, 0.579 mmol, 67%) as a yellow solid.

(2*R*,3*R*,4*S*,5*S*)-5-(2-(4-(2-aminoethyl)phenethylamino)-6-(2,2-diphenylethylamino)-9*H*-purin-9-yl)-*N*-ethyl-3,4-dihydroxytetrahydrofuran-2-carboxamide formate salt

A stirred solution of (3a*R*,4*R*,6*S*,6a*S*)-6-(2-(4-(2-aminoethyl)phenethylamino)-6-(2,2-diphenylethylamino)-9*H*-purin-9-yl)-*N*-ethyl-2,2-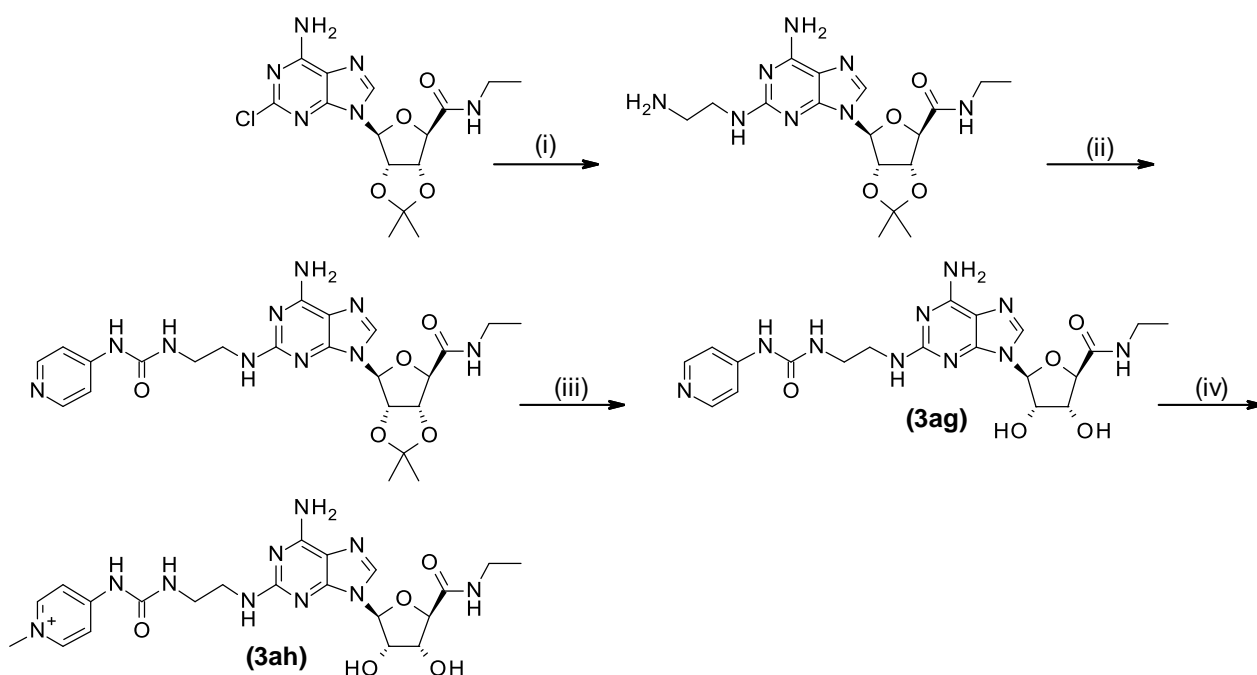dimethyltetrahydrofuro[3,4-*d*][1,3]dioxole-4-carboxamide (0.400 g, 0.579 mmol) in HCl (1 M) (20 mL) was heated to 60°C. After 1 h the mixture was concentrated *in vacuo* and purified by preparative HPLC to give (2*R*,3*R*,4*S*,5*S*)-5-(2-(4-(2-aminoethyl)phenethylamino)-6-(2,2-diphenylethylamino)-9*H*-purin-9-yl)-*N*-ethyl-3,4-dihydroxytetrahydrofuran-2-carboxamide formate salt (0.200 g, 0.287 mmol, 50%) as a white solid.

2-(4-(2-(6-(2,2-diphenylethylamino)-9-((2*S*,3*S*,4*R*,5*R*)-5-(ethylcarbamoyl)-3,4-dihydroxytetrahydrofuran-2-yl)-9*H*-purin-2-ylamino)ethyl)phenyl)-*N*,*N*,*N*-trimethylethanaminium formate

A stirred solution of (2*R*,3*R*,4*S*,5*S*)-5-(2-(4-(2-aminoethyl)phenethylamino)-6-(2,2-diphenylethylamino)-9*H*-purin-9-yl)-*N*-ethyl-3,4-dihydroxytetrahydrofuran-2-carboxamide formate salt (0.100 g, 0.144 mmol, in methanol (15 mL) was treated with potassium carbonate (0.191 g, 1.38 mmol) and iodomethane (1 mL, 16.1 mmol), then heated to 30°C. After 7 h the mixture was concentrated *in vacuo* and purified by preparative HPLC to afford 2-(4-(2-(6-(2,2-diphenylethylamino)-9-((2*S*,3*S*,4*R*,5*R*)-5-(ethylcarbamoyl)-3,4-dihydroxytetrahydrofuran-2-yl)-9*H*-purin-2-ylamino)ethyl)phenyl)-*N*,*N*,*N*-trimethylethanaminium formate (0.050 g, 0.068 mmol, 47%) as a white solid.

Supplemental Scheme 3: (i) ethane-1,2-diamine, 80°C, 3 h, 84%; (ii) 4-isocyanatopyridine, DCM, 0°C – r.t., 1 h; (iii) HCl (1 M), 65°C, 1 h, 49%; (iv) Iodomethane, MeCN, 38°C, 20 h, 80%.

(3a*R*,4*R*,6*S*,6a*S*)-6-(6-amino-2-(2-aminoethylamino)-9*H*-purin-9-yl)-*N*-ethyl-2,2-dimethyltetrahydrofuro[3,4-*d*][1,3]dioxole-4-carboxamide

A stirred mixture of (3a*R*,4*R*,6*S*,6a*S*)-6-(6-amino-2-chloro-9*H*-purin-9-yl)-*N*-ethyl-2,2-dimethyltetrahydrofuro[3,4-*d*][1,3]dioxole-4-carboxamide (0.500 g, 1.31 mmol) and ethane-1,2-diamine (5 mL, 75 mmol) was heated to 80°C for 3 h. The mixture was concentrated *in vacuo* then purified by preparative HPLC to give (3a*R*,4*R*,6*S*,6a*S*)-6-(6-amino-2-(2-aminoethylamino)-9*H*-purin-9-yl)-*N*-ethyl-2,2-dimethyltetrahydrofuro[3,4-*d*][1,3]dioxole-4-carboxamide (0.445 g, 1.09 mmol, 84%) as a solid.

(3a*R*,4*R*,6*S*,6a*S*)-6-(6-amino-2-(2-(3-pyridin-4-ylureido)ethylamino)-9*H*-purin-9-yl)-*N*-ethyl-2,2-dimethyltetrahydrofuro[3,4-*d*][1,3]dioxole-4-carboxamide

A stirred solution of (3a*R*,4*R*,6*S*,6a*S*)-6-(6-amino-2-(2-aminoethylamino)-9*H*-purin-9-yl)-*N*-ethyl-2,2-dimethyltetrahydrofuro[3,4-*d*][1,3]dioxole-4-carboxamide in DCM at 0°C was treated with 4-isocyanatopyridine. The mixture was allowed to wam to room temperature then concentrated *in vacuo* to give a residue which was purified to afford (3a*R*,4*R*,6*S*,6a*S*)-6-(6-amino-2-(2-(3-pyridin-4-
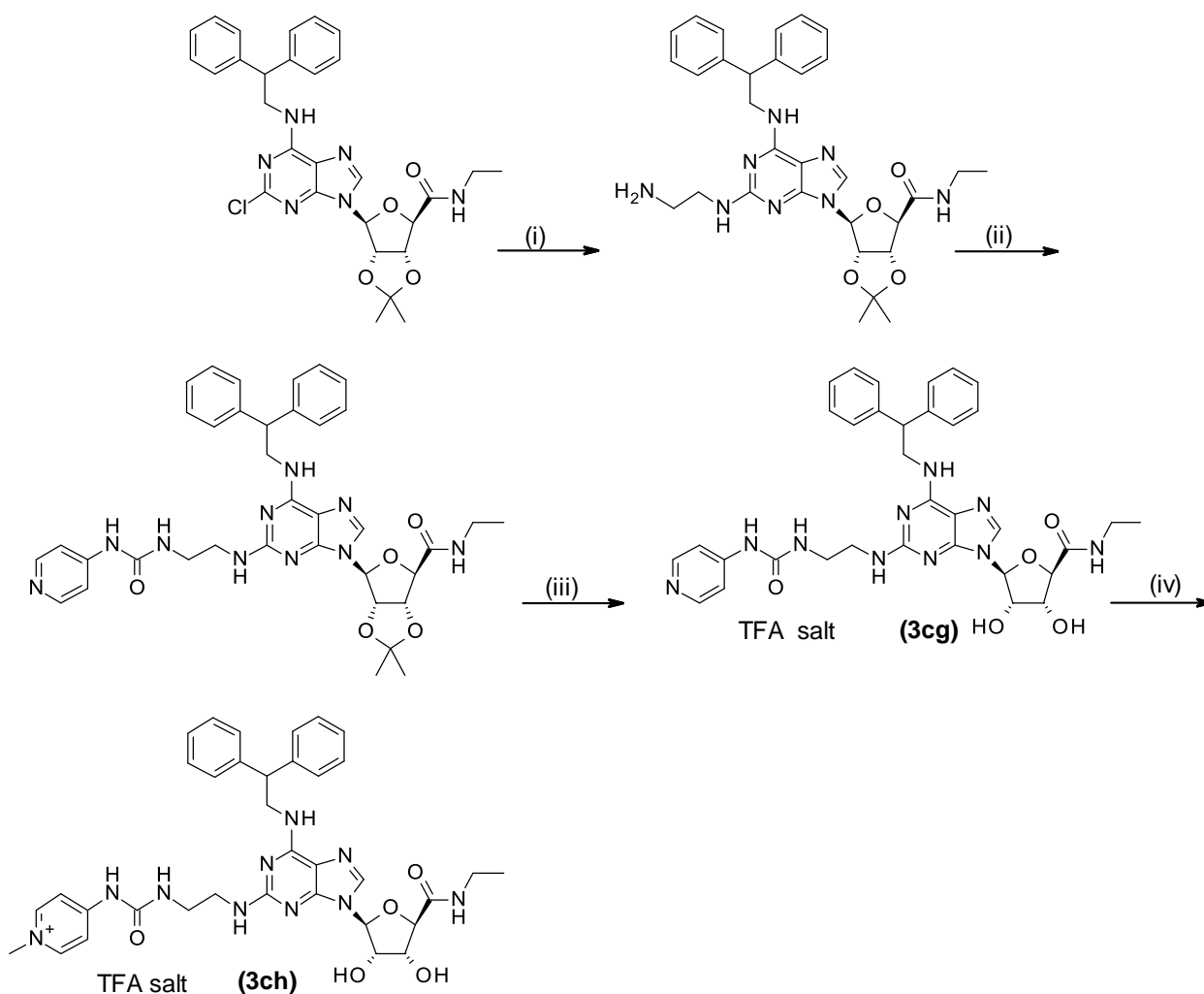
ylureido)ethylamino)-9*H*-purin-9-yl)-*N*-ethyl-2,2-dimethyltetrahydrofuro[3,4-*d*][1,3]dioxole-4-carboxamide as a solid.

(2*R*,3*R*,4*S*,5*S*)-5-(6-amino-2-(2-(3-pyridin-4-ylureido)ethylamino)-9*H*-purin-9-yl)-*N*-ethyl-3,4-dihydroxytetrahydrofuran-2-carboxamide

A stirred solution of (3a*R*,4*R*,6*S*,6a*S*)-6-(6-amino-2-(2-(3-pyridin-4-ylureido)ethylamino)-9*H*-purin-9-yl)-*N*-ethyl-2,2-dimethyltetrahydrofuro[3,4-*d*][1,3]dioxole-4-carboxamide (0.452 g, 0.858 mmol) in HCl (1 M) (2.3 mL) was heated at 65°C for 1 h. The mixture was allowed to cool to room temperature then purified by preparative HPLC to afford (2*R*,3*R*,4*S*,5*S*)-5-(6-amino-2-(2-(3-pyridin-4-ylureido)ethylamino)-9*H*-purin-9-yl)-*N*-ethyl-3,4-dihydroxytetrahydrofuran-2-carboxamide (0.203 g, 0.417 mmol, 49%) as a white solid.

4-(3-(2-(6-amino-9-((2*S*,3*S*,4*R*,5*R*)-5-(ethylcarbamoyl)-3,4-dihydroxytetrahydrofuran-2-yl)-9*H*-purin-2-ylamino)ethyl)ureido)-1-methylpyridinium

A stirred solution of (2*R*,3*R*,4*S*,5*S*)-5-(6-amino-2-(2-(3-pyridin-4-ylureido)ethylamino)-9*H*-purin-9-yl)-*N*-ethyl-3,4-dihydroxytetrahydrofuran-2-carboxamide (0.020 g, 0.041 mmol) in acetonitrile (0.5 mL) was treated with iodomethane (0.1 mL, 1.60 mmol), then heated to 38°C. After 20 h the mixture was concentrated *in vacuo* then purified by preparative HPLC to give 4-(3-(2-(6-amino-9-((2*S*,3*S*,4*R*,5*R*)-5-(ethylcarbamoyl)-3,4-dihydroxytetrahydrofuran-2-yl)-9*H*-purin-2-ylamino)ethyl)ureido)-1-methylpyridinium (0.016 g, 0.033 mmol, 80%) as a solid.

Supplemental Scheme 4: (i) ethane-1,2-diamine, 70°C, 20 h, 61%; (ii) 4-isocyanatopyridine, MeCN, 80°C, 20 h, 96%; (iii) HCl (1 M), 65°C, 1 h, 77%; (iv) Iodomethane, MeCN, MeOH, 35°C, 20 h, 54%.

(3a*R*,4*R*,6*S*,6a*S*)-6-(2-(2-aminoethylamino)-6-(2,2-diphenylethylamino)-9*H*-purin-9-yl)-*N*-ethyl-2,2-dimethyltetrahydrofuro[3,4-*d*][1,3]dioxole-4-carboxamide

A stirred mixture of (3a*R*,4*R*,6*S*,6a*S*)-6-(2-chloro-6-(2,2-diphenylethylamino)-9*H*-purin-9-yl)-*N*-ethyl-2,2-dimethyltetrahydrofuro[3,4-*d*][1,3]dioxole-4-carboxamide (2.99 g, 5.31 mmol) and ethane-1,2-diamine (30 mL, 449 mmol) was heated at 70°C for 20 h. The mixture was concentrated *in vacuo* then purified by flash chromatography (silica), eluting with methanolic aqueous ammonia solution (2%) in DCM, to give (3a*R*,4*R*,6*S*,6a*S*)-6-(2-(2-aminoethylamino)-6-(2,2-diphenylethylamino)-9*H*-purin-9-yl)-*N*-ethyl-2,2-dimethyltetrahydrofuro[3,4-*d*][1,3]dioxole-4-carboxamide (1.89 g, 3.22 mmol, 61%) as a yellow solid.

(3a*R*,4*R*,6*S*,6a*S*)-6-(6-(2,2-diphenylethylamino)-2-(2-(3-pyridin-4-ylureido)ethylamino)-9*H*-purin-9-yl)-*N*-ethyl-2,2-dimethyltetrahydrofuro[3,4-*d*][1,3]dioxole-4-carboxamide

A stirred solution of (3a*R*,4*R*,6*S*,6a*S*)-6-(2-(2-aminoethylamino)-6-(2,2-diphenylethylamino)-9*H*-purin-9-yl)-*N*-ethyl-2,2-dimethyltetrahydrofuro[3,4-*d*][1,3]dioxole-4-carboxamide (1.00 g, 1.70 mmol) in acetonitrile (40 mL) was treated with 4-isocyanatopyridine (0.205 g, 1.71 mmol) then heated to 80°C. After heating for 20 h the mixture was concentrated *in vacuo* to give a residue which was purified by flash chromatography (silica), eluting with methanolic aqueous ammonia solution (2%) in DCM, to afford (3a*R*,4*R*,6*S*,6a*S*)-6-(6-(2,2-diphenylethylamino)-2-(2-(3-pyridin-4-ylureido)ethylamino)-9*H*-purin-9-yl)-*N*-ethyl-2,2-dimethyltetrahydrofuro[3,4-*d*][1,3]dioxole-4-carboxamide (1.16 g, 1.64 mmol, 96%) as a white solid.

(2*R*,3*R*,4*S*,5*S*)-5-(6-(2,2-diphenylethylamino)-2-(2-(3-pyridin-4-ylureido)ethylamino)-9*H*-purin-9-yl)-*N*-ethyl-3,4-dihydroxytetrahydrofuran-2-carboxamide trifluoroacetate salt

A stirred solution of (3a*R*,4*R*,6*S*,6a*S*)-6-(6-(2,2-diphenylethylamino)-2-(2-(3-pyridin-4-ylureido)ethylamino)-9*H*-purin-9-yl)-*N*-ethyl-2,2-dimethyltetrahydrofuro[3,4-*d*][1,3]dioxole-4-carboxamide (0.61 g, 0.86 mmol) in HCl (1 M) (12 mL) was heated at 65°C for 1 h. The mixture was allowed to cool to room temperature then treated with saturated Na_2CO_3 solution until the pH = 7. The mixture was then concentrated *in vacuo* to give a residue which was purified by preparative HPLC to afford (2*R*,3*R*,4*S*,5*S*)-5-(6-(2,2-diphenylethylamino)-2-(2-(3-pyridin-4-ylureido)ethylamino)-9*H*-purin-9-yl)-*N*-ethyl-3,4-dihydroxytetrahydrofuran-2-carboxamide trifluoroacetate salt (0.51 g, 0.65 mmol, 77%) as a white solid.

4-(3-(2-(6-(2,2-diphenylethylamino)-9-((2*S*,3*S*,4*R*,5*R*)-5-(ethylcarbamoyl)-3,4-dihydroxytetrahydrofuran-2-yl)-9*H*-purin-2-ylamino)ethyl)ureido)-1-methylpyridinium trifluoroacetate salt

A stirred solution of (2*R*,3*R*,4*S*,5*S*)-5-(6-(2,2-diphenylethylamino)-2-(2-(3-pyridin-4-ylureido)ethylamino)-9*H*-purin-9-yl)-*N*-ethyl-3,4-dihydroxytetrahydrofuran-2-carboxamide trifluoroacetate salt (0.51 g, 0.65 mmol) in acetonitrile/methanol (20 mL/5 mL) was treated with iodomethane (3 mL, 48.2 mmol), then heated to 35°C. After 20 h the mixture was concentrated *in*

vacuo then purified by preparative HPLC to give 4-(3-(2-(6-(2,2-diphenylethylamino)-9-((2*S*,3*S*,4*R*,5*R*)-5-(ethylcarbamoyl)-3,4-dihydroxytetrahydrofuran-2-yl)-9*H*-purin-2-ylamino)ethyl)ureido)-1-methylpyridinium trifluoroacetate salt (0.279 g, 0.551 mmol, 54%) as a white solid.
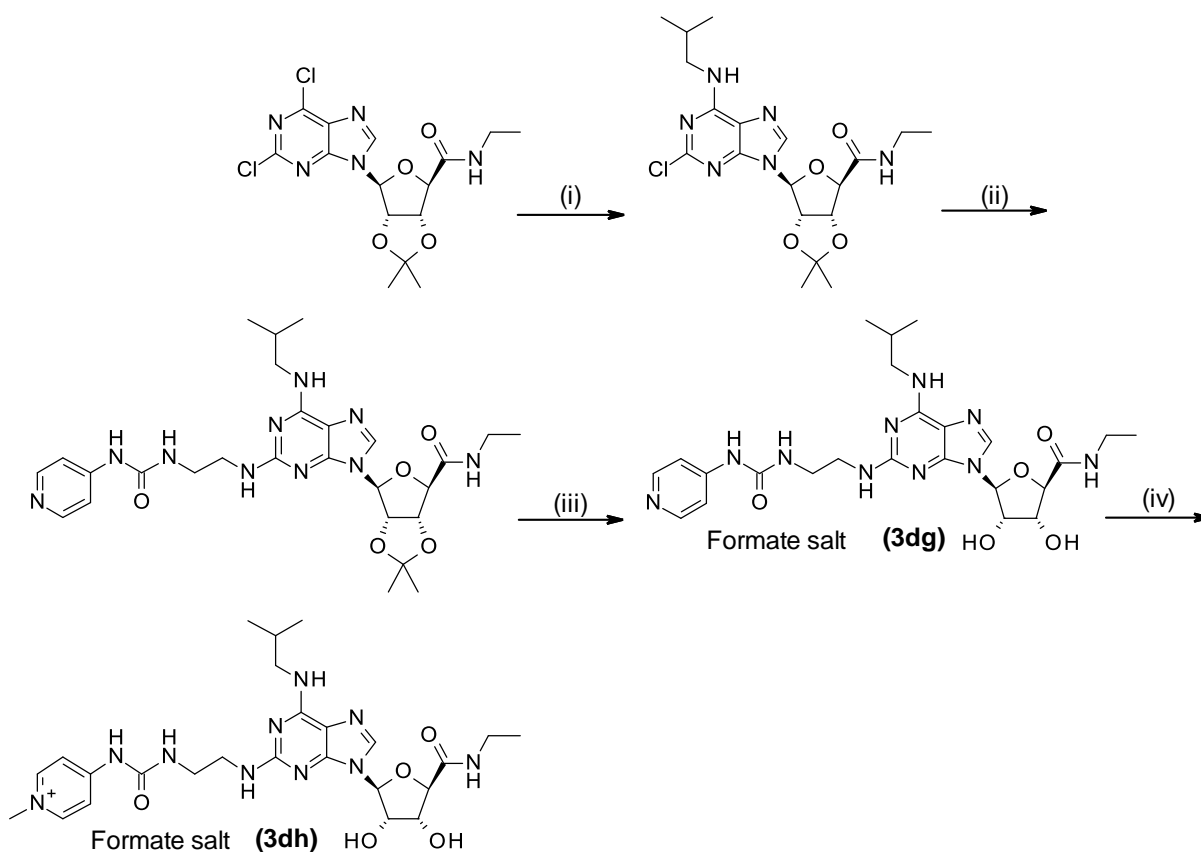
Supplemental Scheme 5: (i) 2-methylpropan-1-amine, EtOH, r.t., 1 h, 55%; (ii) 1-(2-aminoethyl)-3-(pyridin-4-yl)urea, 130°C, 1 h, 30%; (iii) HCl (1 M), 60°C, 1 h, 43%; (iv) Iodomethane, K₂CO₃, MeOH, 35°C, 20 h, 41% (over 2 steps).

(3a*R*,4*R*,6*S*,6a*S*)-6-(2-chloro-6-(isobutylamino)-9*H*-purin-9-yl)-*N*-ethyl-2,2-dimethyltetrahydrofuro[3,4-*d*][1,3]dioxole-4-carboxamide

A stirred mixture of (3a*R*,4*R*,6*S*,6a*S*)-6-(2,6-dichloro-9*H*-purin-9-yl)-*N*-ethyl-2,2-dimethyltetrahydrofuro[3,4-*d*][1,3]dioxole-4-carboxamide (2.0 g, 4.97 mmol) in ethanol (80 mL) was treated with 2-methylpropan-1-amine (2.47 mL, 24.9 mmol). After 1 h at room temperature the mixture was concentrated *in vacuo* then purified by flash chromatography (silica), eluting with methanol in DCM (3%), to afford (3a*R*,4*R*,6*S*,6a*S*)-6-(2-chloro-6-(isobutylamino)-9*H*-purin-9-yl)-*N*-ethyl-2,2-dimethyltetrahydrofuro[3,4-*d*][1,3]dioxole-4-carboxamide (1.20 g, 2.73 mmol, 55%) as a solid.

(3a*R*,4*R*,6*S*,6a*S*)-*N*-ethyl-6-(6-(isobutylamino)-2-(2-(3-pyridin-4-ylureido)ethylamino)-9*H*-purin-9-yl)-2,2-dimethyltetrahydrofuro[3,4-*d*][1,3]dioxole-4-carboxamide

A stirred mixture of (3a*R*,4*R*,6*S*,6a*S*)-6-(2-chloro-6-(isobutylamino)-9*H*-purin-9-yl)-*N*-ethyl-2,2-dimethyltetrahydrofuro[3,4-*d*][1,3]dioxole-4-carboxamide (0.50 g, 1.14 mmol) and 1-(2-aminoethyl)-3-(pyridin-4-yl)urea (1.50 g, 8.32 mmol) was heated at 130°C. After 1 h the mixture was purified by flash chromatography (silica), eluting with methanol in DCM (1%), to give (3a*R*,4*R*,6*S*,6a*S*)-*N*-ethyl-6-(6-(isobutylamino)-2-(2-(3-pyridin-4-ylureido)ethylamino)-9*H*-purin-9-yl)-2,2-dimethyltetrahydrofuro[3,4-*d*][1,3]dioxole-4-carboxamide (0.20 g, 0.34 mmol, 30%) as a solid.

(2*R*,3*R*,4*S*,5*S*)-*N*-ethyl-3,4-dihydroxy-5-(6-(isobutylamino)-2-(2-(3-pyridin-4-ylureido)ethylamino)-9*H*-purin-9-yl)tetrahydrofuran-2-carboxamide formate salt

A stirred solution of (3a*R*,4*R*,6*S*,6a*S*)-*N*-ethyl-6-(6-(isobutylamino)-2-(2-(3-pyridin-4-ylureido)ethylamino)-9*H*-purin-9-yl)-2,2-dimethyltetrahydrofuro[3,4-*d*][1,3]dioxole-4-carboxamide (0.065 g, 0.111 mmol) in HCl (1 M) (4 mL) was heated at 60°C. After 1 h the mixture was concentrated *in vacuo* then purified by preparative HPLC (acetonitrile/water/formic acid [0.05%]) to afford (2*R*,3*R*,4*S*,5*S*)-*N*-ethyl-3,4-dihydroxy-5-(6-(isobutylamino)-2-(2-(3-pyridin-4-ylureido)ethylamino)-9*H*-purin-9-yl)tetrahydrofuran-2-carboxamide formate salt (0.028 g, 0.048 mmol, 43%) as a solid.

4-(3-(2-(9-((2S,3S,4R,5R)-5-(ethylcarbamoyl)-3,4-dihydroxytetrahydrofuran-2-yl)-6-(isobutylamino)-9H-purin-2-ylamino)ethyl)ureido)-1-methylpyridinium formate salt

A stirred solution of (3a*R*,4*R*,6*S*,6a*S*)-*N*-ethyl-6-(6-(isobutylamino)-2-(2-(3-pyridin-4-ylureido)ethylamino)-9*H*-purin-9-yl)-2,2-dimethyltetrahydrofuro[3,4-*d*][1,3]dioxole-4-carboxamide (0.100 g, 0.171 mmol) in HCl (1 M) (6 mL) was heated at 60°C. After 1 h the mixture was concentrated *in vacuo* then the residue dissolved in methanol (10 mL) and treated with potassium carbonate (0.118 g, 0.855 mmol) and iodomethane (0.242 g, 1.70 mmol). The mixture was heated at 35°C for 20 h then concentrated *in vacuo* and purified by preparative HPLC (acetonitrile/water/formic acid [0.05%]) to afford 4-(3-(2-(9-((2S,3S,4R,5R)-5-(ethylcarbamoyl)-3,4-dihydroxytetrahydrofuran-

2-yl)-6-(isobutylamino)-9H-purin-2-ylamino)ethyl)ureido)-1-methylpyridinium formate salt (0.042 g, 0.070 mmol, 41%) as a light yellow solid.
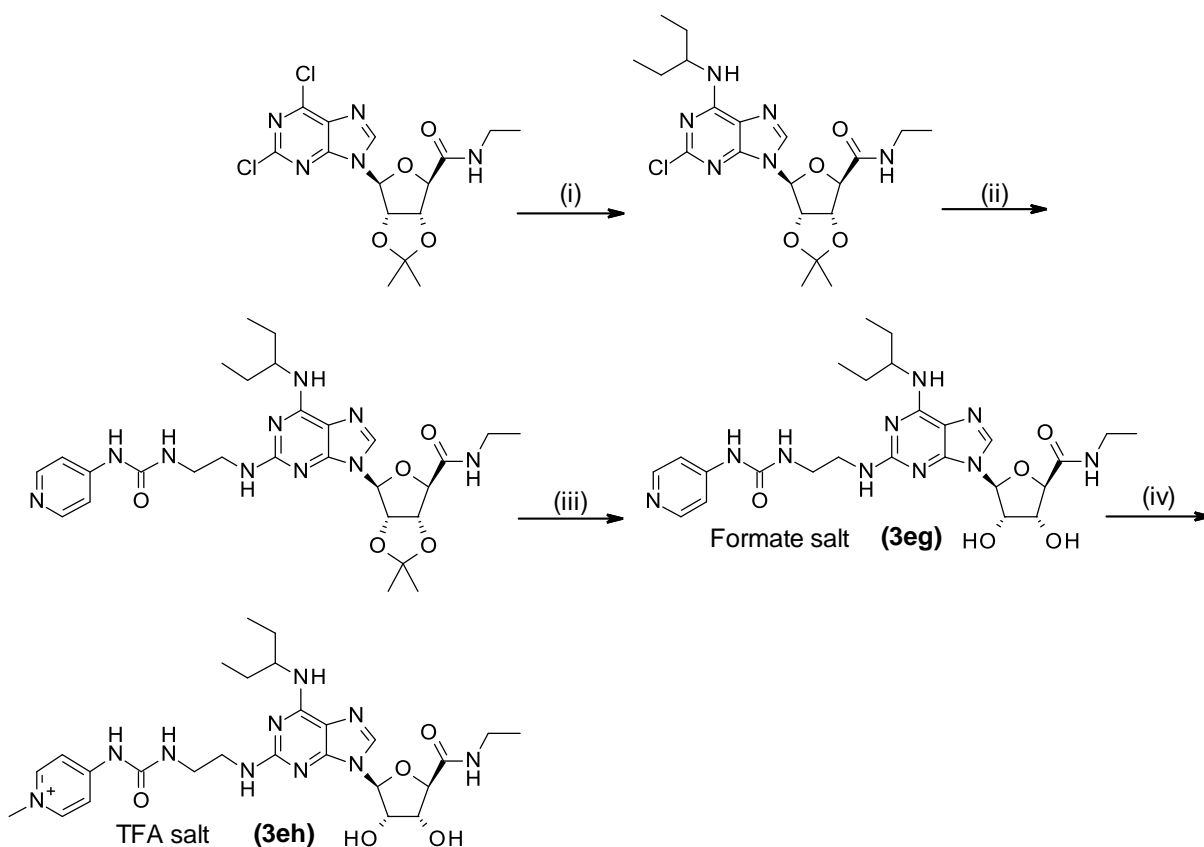
Supplemental Scheme 6: (i) pentane-3-amine, EtOH, r.t., 2 h, 41%; (ii) 1-(2-aminoethyl)-3-(pyridin-4-yl)urea, 130°C, 1 h, 27%; (iii) HCl (1 M), 60°C, 1 h, 23%; (iv) Iodomethane, K₂CO₃, MeOH, 35°C, 20 h, 26%.

(3a*R*,4*R*,6*S*,6a*S*)-6-(2-chloro-6-(pentan-3-ylamino)-9*H*-purin-9-yl)-*N*-ethyl-2,2-dimethyltetrahydrofuro[3,4-*d*][1,3]dioxole-4-carboxamide

A stirred solution of (3a*R*,4*R*,6*S*,6a*S*)-6-(2,6-dichloro-9*H*-purin-9-yl)-*N*-ethyl-2,2-dimethyltetrahydrofuro[3,4-*d*][1,3]dioxole-4-carboxamide (3.0 g, 7.45 mmol) in ethanol (200 mL) was treated dropwise with pentan-3-amine (2.00 mL, 17.16 mmol). After 2 h at room temperature the mixture was concentrated *in vacuo* then purified by flash chromatography (silica), eluting with methanol in DCM (2%), to afford (3a*R*,4*R*,6*S*,6a*S*)-6-(2-chloro-6-(pentan-3-ylamino)-9*H*-purin-9-yl)-*N*-ethyl-2,2-dimethyltetrahydrofuro[3,4-*d*][1,3]dioxole-4-carboxamide (1.40 g, 3.09 mmol, 41%) as a solid.

(3a*R*,4*R*,6*S*,6a*S*)-*N*-ethyl-2,2-dimethyl-6-(6-(pentan-3-ylamino)-2-(2-(3-pyridin-4-ylureido)ethylamino)-9*H*-purin-9-yl)tetrahydrofuro[3,4-*d*][1,3]dioxole-4-carboxamide

A stirred mixture of (3a*R*,4*R*,6*S*,6a*S*)-6-(2-chloro-6-(pentan-3-ylamino)-9*H*-purin-9-yl)-*N*-ethyl-2,2-dimethyltetrahydrofuro[3,4-*d*][1,3]dioxole-4-carboxamide (0.500 g, 1.10 mmol) and 1-(2-aminoethyl)-3-(pyridin-4-yl)urea (1.00 g, 5.55 mmol) was heated at 130°C. After 2.5 h the mixture was allowed to cool to room temperature then purified by flash chromatography (silica), eluting with methanol in DCM (5%), to give (3a*R*,4*R*,6*S*,6a*S*)-*N*-ethyl-2,2-dimethyl-6-(6-(pentan-3-ylamino)-2-(2-(3-pyridin-4-ylureido)ethylamino)-9*H*-purin-9-yl)tetrahydrofuro[3,4-*d*][1,3]dioxole-4-carboxamide (0.27 g, 0.45 mmol, 41%) as a yellow solid.

(2*R*,3*R*,4*S*,5*S*)-*N*-ethyl-3,4-dihydroxy-5-(6-(pentan-3-ylamino)-2-(2-(3-pyridin-4-ylureido)ethylamino)-9*H*-purin-9-yl)tetrahydrofuran-2-carboxamide formate salt

A stirred solution of (3a*R*,4*R*,6*S*,6a*S*)-*N*-ethyl-2,2-dimethyl-6-(6-(pentan-3-ylamino)-2-(2-(3-pyridin-4-ylureido)ethylamino)-9*H*-purin-9-yl)tetrahydrofuro[3,4-*d*][1,3]dioxole-4-carboxamide (0.960 g, 1.61 mmol) in HCl (1 M) (25 mL) was heated at 60°C. After 1 h the mixture was concentrated *in vacuo* then purified by preparative HPLC to afford (2*R*,3*R*,4*S*,5*S*)-*N*-ethyl-3,4-dihydroxy-5-(6-(pentan-3-ylamino)-2-(2-(3-pyridin-4-ylureido)ethylamino)-9*H*-purin-9-yl)tetrahydrofuran-2-carboxamide formate salt (0.220 g, 0.365 mmol, 23%) as a solid.

4-(3-(2-(9-((2*S*,3*S*,4*R*,5*R*)-5-(ethylcarbamoyl)-3,4-dihydroxytetrahydrofuran-2-yl)-6-(pentan-3-ylamino)-9*H*-purin-2-ylamino)ethyl)ureido)-1-methylpyridinium trifluoroacetate salt

A stirred mixture of (2*R*,3*R*,4*S*,5*S*)-*N*-ethyl-3,4-dihydroxy-5-(6-(pentan-3-ylamino)-2-(2-(3-pyridin-4-ylureido)ethylamino)-9*H*-purin-9-yl)tetrahydrofuran-2-carboxamide formate salt (0.200 g, 0.332 mmol), potassium carbonate (0.500 g, 3.62 mmol) and iodomethane (5.0 mL, 80.3 mmol) in methanol (20 mL) was heated at 35°C. After 20 h the mixture was concentrated *in vacuo* and purified by preparative HPLC to afford 4-(3-(2-(9-((2*S*,3*S*,4*R*,5*R*)-5-(ethylcarbamoyl)-3,4-dihydroxytetrahydrofuran-2-yl)-6-(pentan-3-ylamino)-9*H*-purin-2-ylamino)ethyl)ureido)-1-methylpyridinium trifluoroacetate salt (0.060 g, 0.088 mmol, 26%) as a white solid.

Reference List

Palmer TM, Gettys TW, Jacobson KA and Stiles GL (1994) Desensitization of the canine A2a adenosine receptor: delineation of multiple processes. *Molecular pharmacology* **45**(6): 1082-1094.